BIROn - Birkbeck Institutional Research Online

1   # Mechanisms of goethite dissolution in the presence of

2   # desferrioxamine B and Suwannee River fulvic acid at pH 6.5

3

4   Angela G. Stewart[a, b], Karen A. Hudson-Edwards[a] and William E. Dubbin[b*]

5

6

7

8   [a] Department of Earth and Planetary Sciences, Birkbeck, University of London,

9   Malet St., London WC1E 7X, UK

10   [b] Department of Earth Science, The Natural History Museum, Cromwell Road,

11   London SW7 5BD, UK. *Corresponding author. Email: b.dubbin@nhm.ac.uk

12   tel: +44 (0)20-7942-5616

13   fax: +44 (0)20-7942-5537

14

15

16

17

18

19

20   Abstract

21

22   Siderophores are Fe^{3+} specific low MW chelating ligands secreted by micro-

23   organisms in response to Fe stress. Low MW organic acids such as oxalate have been shown

24   to enhance siderophore mediated dissolution of Fe^{3+} oxides. However, the effect of fulvic

25   acid presence on siderophore function remains unknown. We used batch dissolution

26   experiments to investigate Fe release from goethite in the goethite-fulvic acid-

27   desferrioxamine B (goethite-SRFA-DFOB) ternary system. Experiments were conducted at

28   pH 6.5 while varying reagent addition sequence. FTIR and UV-Vis spectroscopy were

29   employed to characterise the Fe-DFOB, Fe-SRFA and DFOB–SRFA complexes. Iron

30   released from goethite in the presence of SRFA alone was below detection limit. In the

31   presence of both SRFA and DFOB, dissolved Fe increased with reaction time, presence of the

32   DFOB-SRFA complex, and where SRFA was introduced prior to DFOB. FTIR data show

33   that in the ternary system, Fe^{3+} is complexed primarily to oxygen of the DFOB hydroxamate

34   group, whilst the carboxylate C=O of SRFA forms an electrostatic association with the

35   terminal NH_3^+ of DFOB. We propose that SRFA sorbed to goethite lowers the net positive

36   charge of the oxide surface, thus facilitating adsorption of cationic DFOB and subsequent

37   Fe^{3+} chelation and release. Furthermore, the sorbed SRFA weakens Fe-O bonds at the

38   goethite surface, increasing the population of kinetically labile Fe. This work demonstrates

39   the positive, though indirect role of SRFA in increasing the bioavailability of Fe^{3+}.

40

41

42

43   Keywords: siderophore, goethite, dissolution, Suwannee River fulvic acid,

44   desferrioxamine

1. INTRODUCTION

In oxic soils and sediments, Fe availability is limited by the low solubility of Fe oxides at circumneutral pH (Raymond and Dertz, 2004). To obtain Fe from these sparingly soluble phases, low MW Fe^{3+}-chelating ligands known as siderophores are released by plants and micro-organisms (Haselwandter, 2008). For example, twice as much Fe is solubilised from goethite in the presence of 126 μM desferrioxamine B (DFOB), a trihydroxamate siderophore, than in the presence of 100 mM HCl at pH 3 over a 28-day reaction (Watteau and Berthelin, 1994). Furthermore, at hydroxamate siderophore concentrations typical of soils (i.e. $10^{-7} – 10^{-8}$ M; Powell et al., 1980), goethite solubility increases over a wide pH range (Kraemer, 2004), where the dissolution of goethite at pH > 4 is described as ligand-controlled (Holmén and Casey, 1996; Reichard et al., 2007a).

Iron(III) is coordinated to the hydroxamate groups of DFOB (Fig. 1) with Fe oxide dissolution influenced by siderophore concentration (Liermann et al., 2000), solution pH (Cervini-Silva, 2008) and temperature (Cocozza et al., 2002). As revealed by single-crystal X-ray diffraction, the chelate molecule consists of two closed loops and a free chain containing a protonated amine (Dhungana et al, 2001). The six hydroxamate oxygen atoms coordinate Fe^{3+} and form a distorted octahedral geometry around the metallic centre (Cozar et al., 2006; Domagal-Goldman et al., 2009) (Fig. 1b). As a consequence of this complexation, the hydroxamate (oxime) protons are lost and the goethite hydroxyl or water groups coordinating Fe^{3+} are displaced.

Iron release from goethite may be enhanced by the presence of low MW organic acids. For example, goethite dissolution by 5×10^{-5} M oxalate, malonate or succinate at pH 6 yielded 10^{-11} M Fe following 400 h reaction (Reichard et al., 2007a) while the presence of citrate produced 10^{-7} M Fe and fumarate yielded undetectable levels of dissolved Fe. When

3

70   DFOB was added to those systems containing both goethite and low MW organic acids,

71   greater amounts of Fe were released than in DFOB-only goethite systems. For example,

72   soluble Fe concentrations increased from 10^{-11} M to 10^{-5} M when 5.0×10^{-5} M DFOB was

73   added to a goethite suspension along with equimolar concentrations of the organic ligands

74   listed above, except for citrate, for which soluble Fe increased only marginally, from 10^{-7} M

75   to 10^{-6} M.

76   Fulvic acid (FA) (Fig. 2), the acid soluble component of humic substances are, along

77   with hydrous Fe oxides and siderophores, ubiquitous in soils and sediments (Stevenson,

78   1985). Fulvic acid sorbs strongly to goethite surfaces at pH values below the point of zero

79   charge for goethite (i.e. < 9.2, Filius et al., 2000). This adsorption involves the formation of

80   inner-sphere complexes via ligand exchange between the oxygen of FA carboxylate groups

81   and the surface oxygen atoms coordinated to Fe at the goethite surface (Filius et al., 2003).

82   Fourier transform infrared (FTIR) spectroscopy confirms the formation of this inner-sphere

83   Fe-fulvate complex by virtue of a shift in the asymmetric carboxylate stretch vibration at pH

84   5 (Fu and Quan, 2006). Humic compounds obtained from various natural environments also

85   complex strongly, and reversibly, with mononuclear Fe, exhibiting stability constants of

86     $10^{21.0}$ to $10^{21.4}$ for Fe-humic complexes isolated from a river plume (Muller and Batchelli,

87   2011), with lower stability constants (i.e. $K = 10^{11.5}$ to $10^{14.0}$) observed for Fe-FA complexes

88   obtained from soil (Pandeya, 1993).

89   Although the effects of low MW acids such as oxalate and citrate on DFOB mediated

90   dissolution of goethite have been examined previously (Reichard et al., 2007a,b), the

91   influence of the higher MW fulvic acid has not yet been explored despite the ubiquity of this

92   humic material in soils and sediments. In this paper we report, for the first time, the results of

93   batch experiments examining the dissolution of goethite in the presence of both Suwannee

94   River fulvic acid (SRFA) and DFOB. The effects of SRFA presence and reagent addition

4

95 sequence were investigated at pH 6.5 to elucidate dissolution mechanisms. The aims of the

96 study were to: (i) determine the effect of SRFA presence on goethite dissolution by DFOB;

97 (ii) develop a mechanistic model of how SRFA influences DFOB function; (iii) characterise

98 possible aqueous Fe-DFOB and Fe-SRFA complexes formed; (iv) propose an overall

99 dissolution mechanism for the goethite-DFOB-SRFA system.

100

101   2. MATERIALS AND METHODS

102

103 2.1. Goethite synthesis and characterisation

104

105   Goethite was synthesised following the method of Schwertmann and Cornell (1991).

106 Briefly, 180 mL of 5 M KOH (Fisher Chemicals, SLR) was rapidly added to 100 mL of 1 M

107 $Fe(NO_3)_3.9H_2O$ (BDH, AnalaR) in a 2 L plastic beaker with constant stirring for 10 min. The

108 suspension was brought to 2 L with ultrapure water (18 MΩ-cm, Milli-Q Millipore) and

109 transferred to five 500 mL amber wide-mouth Nalgene HDPE screw top bottles then aged for

110 24 h at 70 °C (Dubbin and Ander, 2003). The precipitate was washed with ultrapure water

111 through a Büchner funnel into a Büchner flask using Whatman no. 40 filter paper, which was

112 replaced after every 250 mL of suspension to prevent clogging. The precipitate was then

113 allowed to air-dry at 21 °C.

114   The hydroxy Fe precipitates were confirmed as goethite (α-FeOOH) by powder X-ray

115 diffraction (XRD) analyses on an Enraf-Nonius PSD 120, equipped with an INEL 120°

116 curved position sensitive detector utilising Cu Kα_1 radiation (45 kV and 45 mV) at 25 °C. N_2

117 multipoint BET surface area measurements were carried out using a Micrometrics Gemini III

118 2375 instrument. Samples were allowed to de-gas with N_2 at 100 °C for 24 h prior to surface

119 area determination. A kaolinite standard (15.9 ± 0.8 m^2/g) was analysed alongside the

120 goethite samples to monitor accuracy.

121

122 ## 2.2. Batch dissolution experiments

123

124 Stock solutions of: (i) DFOB obtained as the mesylate salt

125 [(C$_{25}$H$_{46}$N$_5$O$_8$NH$_3^+$(CH$_3$SO$_3^-$), MW 656 g mol^{-1}] (Sigma-Aldrich); (ii) SRFA purchased from

126 the International Humic Substance Society [IHSS, Sample 1S101F, MW 1360 g mol^{-1} (Chin

127 et al., 1994)]; and (iii) synthetic goethite (α-FeOOH) were prepared in a combined

128 buffer/electrolyte (MOPS/NaNO$_3$) solution for subsequent use in the batch dissolution

129 experiments. Both DFOB and SRFA were used as received to prepare a 500 μM stock

130 solution of DFOB (0.823 g DFOB dissolved in 250 mL MOPS/NaNO$_3$ solution) and a 65 mg

131 C L^{-1} stock solution of SRFA (0.0624 g SRFA dissolved in 500 mL MOPS/NaNO$_3$ solution).

132 The goethite stock suspension was prepared to a concentration of 1256 mg L^{-1} (3.14 g

133 goethite in 2500 mL MOPS/NaNO$_3$ solution). The combined MOPS/NaNO$_3$ solution

134 consisted of 1 mM 3-(N-morpholino) propanesulfonic acid (MOPS), a non-complexing

135 buffer (Electran VWR BDH PRO LAB molecular biology grade; pH range 6.5 – 7.9; pK$_a$

136 7.2), and 10 mM NaNO$_3$ (BDH AnalaR). The pH of the MOPS/NaNO$_3$ solution was

137 increased from pH 4.5 to 6.5 with the drop-wise addition of 0.1 M NaOH (BDH ARISTAR),

138 continuously monitored with a HANNA Instruments pH meter calibrated at two points (pH

139 4.01 and 7.01). The pH of the goethite suspensions, and DFOB and SRFA solutions, were

140 within the required range therefore no adjustment was required. Solutions and suspensions

141 were stored in amber HDPE wide-mouth screw top bottles to protect from photo-induced

142 reactions and stored at 4 °C to restrict microbial growth. All glassware and plasticware was

143   washed thoroughly with phosphate-free detergent (Decon 90) then rinsed several times with

144   ultra pure water.

145   Fig. 3 shows the reagents, addition sequences, and reaction times for each of the ten

146   batch experiments. For batch experiments 1 through 8 (carried out in duplicate) 90 mL of

147   goethite suspension was dispensed into each of eight 250 mL amber HDPE bottles. One of

148   these eight bottles contained goethite alone (system 8), while a further two bottles without

149   goethite served as procedural blanks to check for adsorption of DFOB (system 9) and SRFA

150   (system 10) onto container walls. Subsequently, 9 mL of DFOB stock solution or 30 mL of

151   SRFA stock solution were added to the bottles (with the exception of systems 3 and 5) as

152   indicated in Fig. 3. The DFOB-SRFA complex was equilibrated for 30 minutes before

153   addition to the goethite suspension (system 6). All batches were brought to a total volume of

154   129 mL with MOPS/NaNO$_3$ and left to equilibrate for 24 h at 25 °C on an orbital shaker

155   (Orbital Incubator SI50) at 100 rpm.

156   Following the initial 24 h contact, further reagents were added as indicated in Fig. 3,

157   brought to final volumes of 168 mL, then placed on the orbital shaker for the duration of the

158   reaction. In systems 3 and 5 we added DFOB and SRFA 4 h before the subsequent addition

159   of, respectively, SRFA and DFOB, to more fully explore the effect of DFOB and SRFA

160   addition sequence. A 4 hour reaction time was chosen because this duration had been

161   reported as the optimal reaction period to achieve ligand adsorption without significant

162   dissolution (Cocozza et al., 2002). The concentration of DFOB, where present, was 270 μM

163   in all batch experiments. The pH of the suspensions in the 250 mL bottles was measured

164   before and after the initial 24 h period, and at the end of the 330 h reaction. In all cases the

165   pH was maintained at 6.5 and did not need further adjusting. Maintaining pH at 6.5 ensured

166   that proton promoted dissolution was negligible. Changes in H$^+$ activity may also influence

167   ligand-controlled goethite dissolution by modifying the concentrations and speciation of

7

168 adsorbed ligands (Reichard et al., 2007b). Subsamples of the suspensions were obtained at

169 intervals throughout the 330 h reaction, then filtered through 25 mm cellulose acetate filters

170 (pore size 0.2 µm) followed by filtration through 25 mm nitrocellulose membrane filters

171 (pore size 0.025 µm) into clear polythene screw cap tubes.

172

173 ## 2.3. Analysis of supernatant solutions

174

175 Five mL portions of the filtrates were acidified with 100 µL 70% HNO_3 (Fisher

176 Scientific) to prevent precipitation of Fe hydroxide then stored at 4 °C. These solutions were

177 analysed for Fe using inductively coupled plasma atomic emission spectroscopy (ICP-AES)

178 analysis (VARIAN VISTA PRO Program ICP Expert version 4.1.0; emission line 259.94 nm;

179 detection limit 89 nmol Fe L^{-1}). Aqueous SRFA and DFOB were quantified by UV-Vis

180 spectroscopy (section 2.5). Total aqueous organic carbon (TOC) was determined by wet

181 combustion with a Shimadzu 5000 TOC analyser after acidification of the filtrate with 10 µL

182 concentrated HCl (BDH ARISTAR). To test the reliability of SRFA quantification by UV-

183 Vis spectroscopy (Gan et al., 2007; Ghabbour and Davies, 2009), aqueous SRFA

184 concentrations were also determined by TOC analysis, subtracting from the total organic C,

185 that C assigned to DFOB as determined by chelometric UV-Vis spectroscopy analysis

186 (section 2.5). Statistical significance among aqueous Fe, DFOB and SRFA concentrations for

187 all batches was determined by applying the unpaired two-tailed Student's t-test with a level of

188 significance of $p = 0.05$. The precipitate retained on each membrane filter following filtration

189 was air-dried at room temperature, placed in an air tight container and preserved for

190 subsequent observation by scanning electron microscopy (SEM), atomic force microscopy

191 (AFM) and FTIR analysis, described below.

192

2.4. FTIR spectroscopy

Synthetic goethite, untreated SRFA and DFOB, and aqueous complexes of SRFA and DFOB prepared in several mole ratios (2:1 Fe^{3+}-DFOB, 5:1 Fe^{3+}-SRFA, 1:1 DFOB-SRFA, and 5:1:1 Fe^{3+}-DFOB-SRFA) were analysed by FTIR. Iron(III) chloride hexahydrate ($FeCl_3.6H_2O$) was used to prepare the Fe^{3+}-complexes. Solid samples for FTIR analysis were obtained from the acidified aqueous complexes by concentrating the solutes through freeze drying (Triad LABCONCO with a JAVAC JL-10 high vacuum pump) to minimise infrared absorption by water and improve peak/band resolution. All samples, including the air-dried residues from filtration, were prepared for FTIR analysis using the KBr pellet technique (Prasad et al., 2006), mixing ~1 mg of sample with 100–200 mg spectroscopy grade KBr (Merck, IR spectroscopy, Uvasol®). When not in use, the pellets were stored in a desiccator to minimise uptake of water. All FTIR data were collected over 200–4000 cm^{-1} on a Perkin Elmer Spectrum One FTIR spectrometer with dedicated spectrum handling software (version 5.0.1). The spectra have a resolution of 4 cm^{-1} and are the aggregate of 128 scans.

2.5. SRFA and DFOB quantification

Filtrate SRFA was quantified by first obtaining a UV-Vis scan (220-900 nm) of a standard aqueous SRFA solution (31.2 mg SRFA L^{-1}) to obtain the λ_{max} (254 nm). A series of aqueous SRFA solutions of varying concentration were then prepared to construct the calibration curve. Aqueous SRFA from each batch dissolution experiment was then determined by placing 1 mL filtrate in micro cuvettes of 10 mm path length and measuring UV absorption at 254 nm (Qu et al., 2003; Tatár et al, 2004). Absorbance readings were obtained on a Shimadzu UV-1800 spectrophotometer fitted with tungsten iodine (visible) and

218   deuterium (UV) lamps. An aliquot of acidified MOPS/NaNO$_3$ was used to base correct the

219   UV-Vis spectrophotometer before analysis of batch solutions.

220   Siderophore concentrations in the filtrates from the adsorption experiments were

221   determined following the chelometric method (Cocozza et al., 2002; Cheah et al., 2003).

222   Spectrophotometric measurements of the Fe-DFOB complex were obtained at 467 nm within

223   1 h after filtration. Filtrates and standards were acidified to pH 1.5 to 1.7 with 8 µL 70%

224   HClO$_4$ (BDH ARISTAR). We then added 170 µL of 15 mM Fe(ClO$_4$)$_3$ to each filtrate sample

225   to give an Fe concentration in excess of that needed to complex all DFOB. Analogous

226   siderophore-free blank solutions containing only MOPS buffer, background electrolyte and

227   added Fe were likewise acidified to pH 1.5 to 1.7. Subtraction of absorbance for the blank

228   solution from that for the sample filtrates yielded the net absorbance, which we attribute to

229   siderophore not adsorbed. The DFOB surface excess (µmol g^{-1}) was determined by dividing

230   the siderophore concentration loss (i.e. 270 µM minus DFOB concentration in the filtrate) by

231   the goethite concentration. DFOB quantification in system 9 (i.e. DFOB without goethite)

232   served as a validation step to account for any DFOB sorbed to container walls and filters.

233   UV-Vis spectra were obtained for DFOB, Fe(ClO$_4$)$_3$, SRFA, Fe^{3+}-DFOB, Fe^{3+}-SRFA,

234   DFOB-SRFA and Fe-DFOB-SRFA standard solutions prepared in a MOPS/NaNO$_3$ matrix

235   and compared to the spectra of the batch filtrate solutions. Furthermore, the spectrum of a

236   MOPS/NaNO$_3$ solution was compared to that of deionized water to ensure that

237   MOPS/NaNO$_3$ peaks did not overlap those from Fe-DFOB.

238

239   2.6. SEM and AFM imaging

240

241   Goethite morphology was determined before and after reaction with SRFA and

242   DFOB. Powdered goethite samples were fixed to Al stubs then coated with Au-Pd prior to

10

243   analysis on a Zeiss Gemini Ultra Plus SEM operating at 5.0 kV and a spot size of 20.00 μm

244   over a range of magnifications to observe gross particle morphology. AFM was used to

245   determine the surface relief of the goethite crystals. The analysis was conducted using an

246   Asylum MFP-3D-SA (Santa Barbara, USA) instrument in AC mode. The prepared film

247   samples (1 cm^2) were placed on glass slides and scanned in air over a 10×10 μm^2 area using

248   an Olympus AC240TS tip (spring constant 2 N m^{-1}). Surface roughness, amplitude and height

249   channels were monitored and analysed using IGOR PRO software.

250

251   <div align="center">3. RESULTS</div>

252

253   3.1. Characterisation of goethite

254

255   The addition of 5 M KOH to 1 M Fe(NO$_3$)$_3$.9H$_2$O produced a brownish-yellow

256   precipitate of Munsell colour 10YR 6/8. The precipitates were confirmed as goethite (α-

257   FeOOH) by comparing their powder X-ray diffraction patterns with those reported in the

258   International Centre for Diffraction Data® Files (ICDD Files 1081-464). All the peaks

259   produced by the precipitates related to the structure of goethite; the absence of extraneous

260   peaks indicated that no other phases were present at detectable levels.

261   Analysis of goethite morphology by SEM showed the crystals to be lathed shaped as

262   observed previously (Cornell et al., 1974; Kosmulski et al., 2004). The fractured appearance

263   of some crystals we attribute to desiccation and water loss under high vacuum. The height of

264   the crystals obtained through AFM analysis was ~ 60 nm, while the N$_2$-BET surface area was

265   43 m^2 g^{-1}, slightly greater than that reported elsewhere (e.g. 35 ± 3 m^2 g^{-1}; Kraemer et al.,

266   1999; 38 m^2 g^{-1}; Carrasco et al., 2007). Sorbed SRFA imparts surface roughness to goethite

267   and disrupts its characteristic lath-shaped morphology.

268

3.2. Goethite dissolution

270

271   Iron release kinetics for goethite dissolution in the presence of DFOB and / or SRFA

272   at 270 μM initial siderophore concentration are shown in Fig. 4. Soluble Fe is detected only

273   for those systems containing both goethite and DFOB (i.e. systems 1 – 6). At reaction times >

274   50 h Fe release broadly followed zero-order kinetics, with Fe concentration depending

275   linearly on time (Table 1). This linearity is commonly observed for far from equilibrium

276   dissolution reactions (Sposito, 1994; Lasaga, 1998), where the slope of the regression line

277   equation (Table 1, column 2) is equal to the zero-order rate coefficient. Generally, goethite

278   suspensions containing both DFOB and SRFA (e.g. systems 4, 5, 6) show increased slopes of

279   the linear fits and greater soluble Fe than those containing only DFOB (i.e. system 1). This

280   observation corroborates the complementary work of Reichard et al. (2007a) on two-ligand

281   systems, who reported increased goethite dissolution at pH 6 in the presence of 50 μM DFOB

282   alongside 50 μM oxalate, malonate, succinate or fumarate. These workers observed that in

283   the presence of 50 μM DFOB alone, goethite dissolution yielded ∼ 5 μM Fe, but this

284   increased to nearly 10 μM Fe with the addition of the above low molecular weight organic

285   ligands. Furthermore, in our study, addition of SRFA prior to DFOB (i.e. systems 4 and 5)

286   yielded greater slopes than for those systems where DFOB was introduced prior to SRFA (i.e.

287   systems 2 and 3). Introduction of the DFOB-SRFA complex to the goethite suspension

288   (system 6) gave rise to the greatest Fe release.

289   In dissolution reactions under far from equilibrium conditions, the zero-order rate

290   coefficient is generally considered to be proportional to either: (i) the specific surface area or

291   (ii) the mass of the dissolving solid (Lasaga, 1998). However, as the normalisation of

292   dissolution rates with respect to surface area is not straightforward (Brantley and Chen,

12

293 1995), we express the dissolution rates with respect to mass of the goethite. Mass normalised

294 rate coefficients ($\mu mol\ g^{-1}\ h^{-1}$) were therefore derived as the slope of the linear fit divided by

295 the goethite mass, and these coefficients are presented in column 3 of Table 1. The mass-

296 normalised dissolution rate coefficients are greatest for those systems containing SRFA,

297 particularly where this humic material was introduced prior to DFOB. Interestingly, the

298 simultaneous introduction of DFOB and SRFA as the DFOB-SRFA complex (system 6)

299 yielded the greatest rate coefficient of all systems.

300 The mass-normalised dissolution rate reported by Cocozza et al. (2002) for the

301 dissolution of goethite by DFOB at 25 °C (i.e. 0.135 $\mu mol\ g^{-1}\ h^{-1}$) is approximately one-half

302 that reported here (i.e. 0.257 $\mu mol\ g^{-1}\ h^{-1}$). Some of this difference may arise from the slightly

303 higher concentration of DFOB used in this study (i.e. 270 μM vs. 240 μM). However, most of

304 this difference in dissolution rate can be attributed to variation in the nature of the goethite

305 sample. Cornell and Schwertmann (2003), for example, cite the influence of goethite

306 morphology and crystallinity as important determinants of dissolution rate. The goethite used

307 in this study was prepared using a method broadly similar to that adopted by Cocozza et al.

308 (2002), with the exception that these earlier workers incorporated a longer aging period

309 yielding a goethite which, presumably, displayed greater long-range order than that used in

310 the present study.

311 UV-Vis spectra for untreated batch filtrates are shown in Fig. 5. These spectra reveal

312 two main regions of absorption: a broad, low peak at 400 – 500 nm which is assigned to Fe^{3+}-

313 DFOB, and another peak at 236 nm which is due to the uncomplexed anionic DFOB species,

314 $HDFOB^{2-}$, whose three hydroxamate groups are deprotonated whilst the terminal amine

315 remains protonated (Edwards et al., 2005). We disregard other causes for the peak at 236 nm

316 as UV-Vis scans of reference solutions of SRFA, $Fe(ClO_4)_3$, $MOPS/NaNO_3$, Fe-DFOB, and

317 Fe-SRFA did not show any absorption in this region. Thus, the spectra in Fig. 5 indicate that

318   the untreated filtrates contain both complexed DFOB as Fe^{3+}-DFOB and uncomplexed

319   DFOB.

320   The values of surface excess of DFOB on goethite at 25 °C, pH 6.5 and 270 μM

321   initial siderophore concentration are given in Table 1 (column 4) for the six systems

322   containing both goethite and DFOB. Although we measure surface excess at a single

323   temperature (i.e. 25 °C) Cocozza et al. (2002) report no significant change in surface excess

324   of DFOB on goethite over the temperature range 25 °C to 55 °C for a comparable system.

325   However, the surface excess we calculate for our system 1 (i.e. 14.4 μmol g^{-1}) is nearly five

326   times that observed by Cocozza et al. (2002) (i.e. 2.99 μmol g^{-1}) under comparable

327   conditions. We again attribute this difference to variation in goethite synthesis procedure,

328   with attendant variation in crystallite morphology and density of reactive surface OH groups

329   (Cornell and Schwertmann, 2003).

330   A pseudo-first-order rate coefficient may be used to characterise the kinetics of

331   ligand-promoted dissolution under far from equilibrium conditions as described by Stumm et

332   al. (1987). This approach was applied by Cocozza et al. (2002) to demonstrate the

333   temperature dependence of DFOB mediated goethite dissolution at 55 °C, and the lack of

334   temperature dependence over the range 25 to 40 °C. For the present study, the coefficient (h^{-}

335   ^{1}) was derived as the ratio of the mass-normalised dissolution rate coefficient to the DFOB

336   surface excess. These values are presented in Table 1 (column 5) and are generally in line

337   with that reported by Kraemer et al. (1999) (i.e. 0.01 h^{-1}). This broad congruence of pseudo-

338   first-order rate coefficients implies that differences in dissolution rate depend principally on

339   DFOB surface excess as influenced by reagent addition sequence.

340

341   3.3. FTIR spectra

342

343   The dominant FTIR vibrations and corresponding assignments for the Fe-free and

344   Fe^{3+}-complexed standards are shown in Table 2. All FTIR absorption peaks produced by our

345   synthetic goethite relate to the structure of goethite. The absence of extraneous peaks

346   indicated that no other phases were present at detectable levels. The FTIR spectrum for our

347   synthetic goethite (Fig. 6) has an absorption band at 640 cm^{-1}, representing the FeO_6 lattice

348   vibrations (Prasad et al., 2006). Other prominent vibrations are the in-plane (δ) and out-of-

349   plane (γ) deformational (bending) modes of hydroxyls at 891 cm^{-1} and 795 cm^{-1}, respectively

350   (cf., Prasad et al. 2006). The broad absorption band located at 3132 cm^{-1} is assigned to the

351   hydroxyl stretch of surface OH, previously reported at $3100 - 3150$ cm^{-1} (Cornell and

352   Schwertmann, 2003).

353   In the FTIR spectrum for DFOB the terminal N-H stretching vibrations occur at 3128

354   cm^{-1} and 3325 cm^{-1}, while the vibrational stretching of the amide I band of the C=O group

355   occurs at 1624 cm^{-1} (Cozar et al., 2006; Siebner-Freibach et al., 2006). Another C=O

356   absorption band at 1599 cm^{-1} represents the hydroxamate C=O (cf., Edwards et al., 2005;

357   Domagal-Goldman et al., 2009). An absorption band at 1537 cm^{-1} arises from the

358   superposition of N-H bending and C-N stretching vibrations in the amide II group (cf.,

359   Nightingale and Wagner, 1954) as well as O-H (hydroxamate) in-plane bending vibrations

360   (Cozar et al., 2006). The band at 1480 cm^{-1} is assigned to both the hydroxamate NOH bend

361   and the C-N oxime (hydroxamate resonance structure) stretch corresponding to the 1470 cm^{-1}

362   band of Edwards et al. (2005) (Fig. 6). We also observed a band at 1386 cm^{-1} arising from a

363   combination of vibrational deformation modes in the hydroxamate group and terminal N (cf.,

364   1379 cm^{-1} Edwards et al., 2005). An additional band, at 1047 cm^{-1}, coincides with the

365   hydroxamate N-O resonance of DFOB. However, this band is not due exclusively to DFOB

366   as methanesulfonate, the counter-ion of the DFOB mesylate salt, also shows strong

367   absorption at 1049 cm^{-1} (Borer et al., 2009; Simanova et al., 2010).

15

368   The FTIR spectrum for SRFA (Fig. 6) displayed two prominent absorption bands, at

369   3425 cm^{-1} and 1720 cm^{-1}, and these were assigned to the phenolic O-H and protonated

370   carboxylic acid C=O vibrational stretching modes, respectively (cf., International Humic

371   Substance Society, 2008). Other absorption bands at 1629 cm^{-1} and 1384 cm^{-1} represent,

372   respectively, the deprotonated asymmetric and symmetric vibrational stretching of

373   carboxylate C=O (cf., Fu and Quan, 2006; Hay and Myneni, 2007). The broad band at 1218

374   cm^{-1}, assigned to the O-H phenolic stretch, was previously observed at 1217 cm^{-1} by Fu and

375   Quan (2006).

376   Complexation between DFOB and Fe^{3+} yields a shift in the amide I band to 1622 cm^{-1}

377   from 1624 cm^{-1} (Fig. 6) as reported by Edwards et al. (2005). The hydroxamate absorption

378   bands at 1537 cm^{-1} and 1480 cm^{-1}, as well as the absorption band at 1386 cm^{-1}, assigned to

379   the hydroxamate near the terminal N, also disappeared upon complexation of DFOB to Fe^{3+}.

380   The Fe^{3+}-DFOB complex gave rise to a new vibrational stretching mode at 1568 cm^{-1},

381   assigned to hydroxamate C=N, and a shift of the existing 1047 cm^{-1} band to 1045 cm^{-1},

382   assigned to hydroxamate N-O (Fig. 6) (Cozar et al., 2006). Upon coordination of

383   hydroxamate oxygen to Fe^{3+}, a new hydroxamate absorption band emerged at 1459 cm^{-1},

384   previously reported at 1455 cm^{-1} by Borer et al. (2009), in a region where bands at 1537 cm^{-1}

385   and 1480 cm^{-1} once appeared (Table 2). The Fe^{3+}-DFOB complex also gives rise to a band at

386   561 cm^{-1}, reported previously at 555 cm^{-1} (Cozar et al., 2006), attributed to the Fe-O

387   stretching vibration, but distinct from the Fe-O stretching of the goethite lattice. Additionally,

388   a broad and intense peak at 3368 cm^{-1}, accompanied by two small shoulders, we attribute to

389   the dissociation of the hydroxamate hydroxyl groups following Fe^{3+} coordination.

390   Following complexation of Fe^{3+} with SRFA, the O-H band at 3425 cm^{-1} becomes

391   broader, and shifts to 3410 cm^{-1} (Fig. 6). In contrast, the COOH and asymmetric C=O bands

392   at 1720 cm^{-1} and 1629 cm^{-1}, respectively, disappeared, whilst new, slightly lower intensity

393   bands appeared at 1687 cm^{-1} and 1631 cm^{-1}. Meanwhile, the peak at 1384 cm^{-1} became

394   sharper and more intense following Fe^{3+} complexation with SRFA (cf., Fu and Quan, 2006),

395   indicating the complexation of carboxylate oxygen to Fe^{3+}.

396   Our FTIR assignments for the DFOB-SRFA and Fe^{3+}-DFOB-SRFA complexes are

397   based on comparison of the FTIR spectra for DFOB, SRFA, Fe^{3+}-DFOB, Fe^{3+}-SRFA, DFOB-

398   SRFA and Fe^{3+}-DFOB-SRFA. Upon formation of the DFOB-SRFA complex, the SRFA

399   phenolic absorption band at 3425 cm^{-1} becomes less intense and slightly broader, shifting to

400   3417 cm^{-1}, while another phenolic band at 1216 cm^{-1} shifted to 1218 cm^{-1} (Fig. 6). The

401   intensity of the prominent SRFA carboxylic C=O band at 1720 cm^{-1} decreased significantly

402   and shifted to 1719 cm^{-1}, whilst the asymmetric C=O band at 1629 cm^{-1} shifted to 1626 cm^{-1}.

403   With respect to the DFOB, bands assigned to the terminal amines shifted from 3128 cm^{-1} and

404   3325 cm^{-1} to a single band at 2939 cm^{-1} of lower intensity.

405   Formation of the Fe^{3+}-DFOB-SRFA complex changed the FTIR spectra for both

406   SRFA and DFOB (Fig. 6). The intensity of the SRFA carboxylic C=O band was reduced,

407   shifting from 1720 to 1723 cm^{-1}, while the SRFA symmetric C=O absorption band at 1384

408   cm^{-1} disappeared. The SRFA phenolic OH band at 1216 cm^{-1} remained largely as it was in

409   the DFOB-SRFA complex, whilst the asymmetric stretching of the carboxylate C=O

410   increased from 1629 cm^{-1} in the Fe-free complex to 1642 cm^{-1} in the Fe^{3+}-DFOB-SRFA

411   complex. The phenolic OH band shifted from 3425 cm^{-1} for the Fe-free SRFA to 3437 cm^{-1}

412   for the Fe^{3+}-DFOB-SRFA complex. The N-O resonance of the hydroxamate group decreased

413   from 1047 cm^{-1} in DFOB to 1042 cm^{-1} in the Fe^{3+}-DFOB-SRFA complex and was

414   accompanied by considerable peak sharpening. Furthermore, the Fe-O vibration at 561 cm^{-1}

415   indicating complexation between Fe^{3+} and DFOB was observed at 542 cm^{-1} in the ternary

416   complex (Fig. 6). Weak bands at 3010 cm^{-1} and 2954 cm^{-1} for the Fe^{3+}-DFOB-SRFA

417   complex are likely due to the decrease in frequency of the N-H group of the terminal N in the

418   DFOB as a result of electrostatic interaction between the DFOB terminal amine and charged

419   SRFA groups.

420

421   <div align="center">4. DISCUSSION</div>

422

423   4.1. Sorption of SRFA and DFOB to goethite

424

425   Adsorption of organic matter to iron oxide surfaces occurs by electrostatic

426   interactions, ligand exchange, hydrogen bonding and van der Waals interactions (Sposito,

427   1984). Coulombic attraction of organic solutes to metal oxides can be predicted through

428   construction of a Schindler diagram, a banded rectangle in which the charge properties of the

429   adsorptive and adsorbent are compared as a function of solution pH (Fig. 7) (Schindler,

430   1990). The bottom rectangle displays a horizontal line indicating the pH range over which

431   adsorption is expected to occur based solely on charge. Adsorption occurring outside of this

432   range implies the involvement of specific adsorption mechanisms. On the basis of the

433   Schindler diagram depicted in Fig. 7a, adsorption of SRFA to goethite is predicted over pH ~

434   3 to 9.

435   At pH 6.5 and an initial SRFA concentration of 11.6 mg C L^{-1}, the surface excess of

436   SRFA on goethite was 0.33 mg m^{-2}. This value compares favourably with that reported by

437   Filius et al. (2000) for fulvate adsorption to goethite at pH 7 (i.e. 0.3 mg FA g^{-1}) and also

438   Weng et al. (2006) for their system at pH 5.5 (i.e. 0.4 mg FA g^{-1}). FTIR spectra for the

439   goethite-SRFA surface association were too complex to derive useful molecular-level

440   information concerning adsorption mechanisms. However, FTIR spectra for aqueous Fe^{3+}-

441   SRFA species, when compared with spectra for several reference aqueous complexes (Fig.

442   6), revealed that Fe^{3+} forms inner-sphere complexes with COOH and phenolic OH of SRFA,

<div align="center">18</div>

443   consistent with that reported in previous studies (Fu and Quan, 2006; Hay and Myeni, 2007).

444   Furthermore, application of the charge distribution multi-site complexation (CD-MUSIC)

445   model provides theoretical evidence that carboxylic groups of SRFA form inner-sphere

446   complexes with Fe via the singly coordinated surface hydroxyls of goethite (i.e. those

447   hydroxyls coordinated to a single Fe^{3+} cation) (Weng et al., 2005; Weng et al., 2006). On the

448   basis of these theoretical predictions and our experimental data, we propose that SRFA binds

449   to the goethite surface via inner-sphere complexation as depicted in Fig. 8, corroborating the

450   work of Filius et al. (2000), who observed inner-sphere adsorption of fulvic acid at pH below

451   the PZC for goethite. Importantly, SRFA adsorption lowers the PZC of goethite and reduces

452   positive surface charge in the vicinity of the adsorption site (Tipping and Cooke, 1982).

453   The Schindler diagram shown in Fig. 7b predicts that goethite can serve as an

454   effective sorbent for DFOB only at pH ~ 8 to 9. However, for our systems at pH 6.5, we

455   observe a surface excess of DFOB ranging from 14.4 to 26.5 μmol g^{-1} (Table 1). Much of this

456   DFOB will be adsorbed via inner-sphere surface complexes (Carrasco et al., 2007), however

457   electrostatic factors may be significant in increasing overall uptake. The predicted

458   electrostatic repulsion at pH 6.5 between DFOB (pK$_a$ ~ 8.6) and the positively charged

459   goethite surface (PZC = 9.2) can be minimised through orientation of the approaching

460   siderophore such that the hydroxamate group furthest from the protonated amine makes first

461   contact with the surface (Cocozza et al., 2002). More significantly, adsorption of the anionic

462   SRFA reduces the positive surface charge of goethite near the site of adsorption (Tipping and

463   Cooke, 1982), thus facilitating localised uptake of DFOB. Consistent with the predicted

464   SRFA enhanced uptake of DFOB, our data show that those systems with both SRFA and

465   DFOB give rise to greater DFOB surface excess than system 1, which contains only DFOB

466   (Table 1).

467

4.2. Aqueous complexes

UV-Vis spectroscopic analysis confirmed the presence of the Fe^{3+}-DFOB complex in supernatant solutions from batch dissolution experiments (Fig. 5). The emergence of FTIR absorption bands at 1459 cm^{-1} and 561 cm^{-1}, assigned to Fe-O (Table 2; Fig. 6), following formation of the Fe^{3+}-DFOB complex provides evidence for presence of the Fe-hydroxamate bond as depicted in Fig. 1b. These observations are consistent with predictions based on the high affinity of desferrioxamine B for the Fe^{3+} cation ($K = 10^{31}$) (Kraemer, 2004).

The absence of both soluble Fe and the Fe^{3+}-SRFA species in the supernatant solutions of system 7 indicates that goethite dissolution does not occur at detectable levels in the presence of SRFA alone at pH 6.5 (Fig. 4). However, FTIR analysis of model compounds reveals the diagnostic absorption bands that indicate presence of the Fe^{3+}-SRFA complex, a species that may well form following the liberation of Fe^{3+} by DFOB. The most significant FTIR band arising from the complexation of SRFA with Fe is due to changes in the carboxylate C=O vibration, appearing at 1687 cm^{-1} in Fe^{3+}-SRFA and 1720 cm^{-1} in Fe-free SRFA. Fu and Quan (2006) observed similar changes in C=O vibrations when FA was sorbed to haematite. The other functional group indicative of Fe^{3+}-SRFA bonding, the phenolic OH, changes from 3425 cm^{-1} in the uncomplexed SRFA to 3410 cm^{-1} for Fe^{3+}-SRFA (Table 2).

Localisation of Fe within the ternary Fe-DFOB-SRFA complex can help to reveal the mechanisms of goethite dissolution when both organic ligands are present. The FTIR absorption band most diagnostic of Fe complexation by SRFA arises from the carboxylate C=O vibration which, when complexed to Fe, decreases from 1720 cm^{-1} to 1687 cm^{-1}. In the ternary complex this vibration occurs at 1723 cm^{-1} (Table 2), broadly similar to that of the Fe-free SRFA. Furthermore, we observe the main band representing the Fe^{3+}-DFOB complex, the Fe-O vibration, is also present for the Fe-DFOB-SRFA complex, although

493   occurring at the somewhat lower frequency of 542 cm^{-1}. On the basis of these spectroscopic

494   observations we infer that Fe in the ternary complex is bound only to the hydroxamate groups

495   of DFOB. Thus, in the presence of both DFOB and SRFA, dissolved Fe^{3+} is complexed by

496   DFOB rather than SRFA, consistent with our observations, and as predicted by the much

497   higher affinity of Fe^{3+} for DFOB than for SRFA at pH 6.5 (Pandeya, 1993; Kraemer, 2004;

498   Muller and Batchelli, 2011). The FTIR spectrum for Fe-DFOB-SRFA also shows notable

499   increases in wavenumber for SRFA phenolic OH (3437 cm^{-1}) and C=O (1642 cm^{-1}),

500   compared to their uncomplexed form (Table 2). However, we believe these wavenumber

501   shifts are not due to Fe complexation by SRFA but rather to ring strain caused by a change in

502   SRFA conformation to accommodate the DFOB molecule as the Fe-O complex forms

503   (Sharma, 2007).

504   FTIR data show that SRFA and DFOB combine to form intimate associations in

505   aqueous solution. Specifically, bonding between the SRFA phenolic OH and the residual

506   positive charge on the DFOB terminal NH_3 group yields a significant wavenumber change

507   for these groups, shifting the uncomplexed SRFA phenolic OH from 3425 cm^{-1} to 3417 cm^{-1}

508   in the DFOB-SRFA complex (Table 2). Curiously, the SRFA phenolic OH appears to

509   dominate these associations, despite the greater population of carboxyl groups within this

510   humic material, with reports of carboxyl:phenol molar ratios varying from 3:2 (Alvarez-

511   Puebla et al., 2006) to 4:1 (Ritchie and Perdue, 2003). The FTIR bands for the DFOB

512   terminal NH_3 group vibrations display even greater wavenumber shifts, from 3128 cm^{-1} and

513   3325 cm^{-1} in the uncomplexed siderophore to a single absorption peak at 2939 cm^{-1} in the

514   DFOB-SRFA complex.

515

516   4.3. Influence of DFOB and SRFA on goethite dissolution

517

518   DFOB adsorbs to goethite principally via inner-sphere surface complexes (Carrasco et

519   al., 2007), the necessary first step in ligand-controlled dissolution. The rate law for ligand-

520   controlled dissolution predicts that the mass-normalised dissolution rate of goethite, R_{DFOB},

521   will be proportional to the DFOB surface excess, n_{DFOB}:

522

523                         $$R_{DFOB} = k_{DFOB}\, n_{DFOB}$$

524

525   where k_{DFOB} is a pseudo first-order rate coefficient. The dissolution of goethite by

526   siderophores obeys this rate law under many experimental conditions, even in the presence of

527   low MW organic ligands such as oxalate (Cheah et al., 2003). Our values for k_{DFOB} show

528   little variation irrespective of treatment ($0.012 - 0.020$ h^{-1}) (Table 1, column 5) and are

529   broadly in line with that reported by Kraemer et al. (1999) (i.e. 0.01 h^{-1}). However, the

530   pseudo first-order rate coefficient for dissolution of goethite by DFO-D1, the acetyl

531   derivative of DFOB, increases to 0.05 h^{-1} (Kraemer et al., 1999) while that for a simple

532   monohydroxamate ligand, acetohydroxamic acid, was calculated as 0.073 h^{-1} (Holmén and

533   Casey, 1998).

534   In the present study, Fe release from goethite increased with the addition of SRFA,

535   particularly where SRFA is added prior to DFOB (systems 4 and 5), and further still when

536   SRFA is introduced as the DFOB-SRFA complex (system 6) (Fig. 4). A quantitative

537   assessment of the effect of SRFA presence on goethite dissolution can obtained through

538   comparison of the mass-normalised zero-order rate coefficients (Table 1, column 3). The rate

539   coefficients for systems 4 (0.364 μmol g^{-1} h^{-1}) and 5 (0.412 μmol g^{-1} h^{-1}) are 40 to 60% larger

540   than that for system 1 (0.257 μmol g^{-1} h^{-1}), while the coefficient for system 6 (0.440 μmol g^{-1}

541   h^{-1}) is nearly 70% larger than for the SRFA-free system.

542   Despite the positive influence of SRFA on goethite dissolution by means of increased

543   adsorption of DFOB (compare DFOB surface excess for system 1 with that for systems 2 – 6;

544   Table 1, column 4), the rate of Fe release does not correlate linearly with DFOB surface

545   excess. This nonlinear relationship between DFOB adsorption and goethite dissolution may

546   reflect changes in surface speciation of DFOB when SRFA is present. The SRFA induced

547   reduction in positive surface charge enables greater electrostatic adsorption of DFOB as

548   predicted by Tipping and Cooke (1982). However, as formation of a DFOB inner-sphere

549   complex is the required first step in ligand-controlled dissolution of goethite, DFOB held

550   non-specifically through Coulombic forces would not contribute to goethite dissolution.

551   Furthermore, in the case of system 6, inner-sphere complexation of DFOB to goethite may be

552   partly limited by the rate at which DFOB and SRFA decouple. Nevertheless, the effect of

553   SRFA presence on the DFOB-goethite system has important implications for the microbial

554   acquisition of Fe in soils and other humic rich environments. Data in Fig. 4 show that for

555   nearly all systems the efficacy of DFOB is increased with SRFA presence. For example, at

556   reaction times of 120 and 330 h, system 1 (with only DFOB) yields 34.7 and 70.3 μM Fe

557   while system 6 (containing both DFOB and SRFA) yields 71.6 and 125.7 μM Fe,

558   respectively (Fig. 4). Thus, the benefit to the microbe producing the siderophore is

559   substantial, and this advantage is achieved with little or no energetic cost to the organism.

560

561   4.4. Mechanism of SRFA enhanced goethite dissolution

562

563   Various mechanisms have been proposed to explain the effect of low MW organic

564   acids on goethite dissolution by DFOB. For example, in their examination of the oxalate-

565   DFOB-goethite system at pH 5, Cheah et al. (2003) suggest that Fe solubilised from the

566   goethite surface by oxalate is subsequently wrested from the Fe^{3+}-oxalate aqueous complex

567   by DFOB. Given sufficient DFOB to complex soluble Fe, oxalate will thus be liberated to

568   react once again with the goethite surface. Reichard et al. (2007a), also examining the

569   oxalate-DFOB-goethite system, proposed a dissolution mechanism broadly similar to that of

570   Cheah et al. (2003), except that the former workers identified two distinct pools of labile Fe,

571   namely, (i) Fe^{3+} present as a residuum of goethite synthesis and (ii) kinetically labile Fe^{3+}

572   coordinated to unshared hydroxyls. The mechanism we propose here for the dissolution of

573   goethite in the presence of DFOB and the higher MW organic compound, SRFA, differs from

574   those proposed for oxalate in that SRFA plays a largely indirect, though no less important

575   role in increasing the efficacy of DFOB. Adsorbed SRFA reduces the net positive surface

576   charge of goethite, thereby increasing DFOB uptake, and also, through formation of Fe

577   complexes with fulvic carboxyl and phenol groups, increases the pool of labile surface Fe.

578   Our model for goethite dissolution by DFOB in the presence of SRFA, illustrated in Fig. 9, is

579   summarised below:

580

581   (i) surface Fe of goethite is coordinated to SRFA via carboxylic $(GOE)Fe^{3+}$-$^{-}OOC(SRFA)$ or

582   phenolic $(GOE)Fe^{3+}$-$^{-}O(SRFA)$ functional groups through ligand exchange;

583

584   (ii) the Fe^{3+}-SRFA attachment destabilises Fe-O bonds at the goethite surface, leading to

585   labilisation of Fe^{3+};

586

587   (iii) adsorbed SRFA locally reduces the positive charge on the goethite surface, thereby

588   enhancing $DFOB^{+}$ uptake;

589

590   (iv) protons are displaced from the hydroxamate groups of DFOB as these groups bind to the

591   labile Fe^{3+} via ligand exchange;

24

592

593   (vi) the Fe^{3+}-$DFOB^+$ complex is released to solution where it remains a free species or

594   subsequently complexes with aqueous SRFA.

595

<div align="center">5. CONCLUSIONS</div>

597

598   Our results show that dissolution of goethite by DFOB is enhanced considerably

599 through the presence of FA, particularly when FA sorption preceeds that of DFOB, or when

600 the two organic compounds are sorbed simultaneously. Importantly, our batch dissolution

601 experiments incorporating FA reveal a more complex picture of siderophore function than is

602 portrayed in the current literature. This humic material is revealed as a catalyst for goethite

603 dissolution, in the sense that FA enhances the efficacy of DFOB but is itself not directly

604 involved in Fe solubilisation. This work shines important new light on the factors influencing

605 Fe acquisition by microorganisms and plants in soils and sediments, environments in which

606 humic materials are ubiquitous. The incorporation of natural organic matter such as FA into

607 geochemical models of siderophore function is therefore essential to more accurately predict

608 the geochemical cycling of Fe in these natural environments.

609

610

617   for SEM analysis and photography, Superb Misra for AFM analysis and photography, and

618   Jens Najorka for XRD analysis.

619

620   R E F E R E N C E S

621

622   Alvarez-Puebla R.A., Valenzuela-Calahorro C. and Garrido J.J. (2006) Theoretical study on

623   fulvic acid structure, conformation and aggregation - A molecular modelling approach.

624   *Sci. Total Environ.* 358, 243–254.

625   Borer P., Hug S.J., Sulzberger B., Kraemer S.M. and Kretzschmar R. (2009) ATR-FTIR

626   spectroscopic study of the adsorption of desferrioxamine B and aerobactin to the surface

627   of lepidocrocite (γ-FeOOH). *Geochim.Cosmochim. Acta* 73, 4661-4672.

628   Brantley S.L. and Chen Y. (1995) Chemical weathering rates of pyroxenes and amphiboles.

629   *Rev. Mineral.* 31, 119-172.

630   Carrasco N., Kretzschmar R., Pesch M.-L. and Kraemer S.M. (2007) Low concentrations of

631   surfactants enhance siderophore-promoted dissolution of goethite. *Environ. Sci. Technol.*

632   41, 3633-3638.

633   Cervini-Silva J. (2008) Adsorption of trihydroxamate and catecholate siderophores on alpha-

634   iron (hydr)oxides and their dissolution at pH 3.0 to 6.0. *Soil Sci. Soc. Am. J.* 72, 1557-

635   1562.

636   Cheah S., Kraemer S.M., Cervini-Silva J. and Sposito G. (2003) Steady-state dissolution

637   kinetics of goethite in the presence of desferrioxamine B and oxalate ligands: implications

638   for the microbial acquisition of iron. *Chem. Geol.* 198, 63-75.

639   Chin Y., Aiken G. and O'Loughlin E. (1994) Molecular weight, polydispersity, and

640   spectroscopic properties of aquatic humic substances. *Environ. Sci. Technol.* 28, 1853–

641   1858.

26

642   Cocozza C., Tsao C.C.G., Cheah F., Kraemer S.M., Raymond K.N., Miano T.M. and Sposito

643   G. (2002) Temperature dependence of goethite dissolution promoted by trihydroxamate

644   siderophores. *Geochim.Cosmochim. Acta* 66, 431-438.

645   Colnaghi Simionato A.V., Cantú M.D. and Carrilho E. (2006) Characterization of metal-

646   deferroxamine complexes by continuous variation method: A new approach using

647   capillary zone electrophoresis. *Microchem. J.* 82, 214-219.

648   Cornell R.M., Posner A.M. and Quirk J.P. (1974) Crystal morphology and the dissolution of

649   goethite. *J. Inorg. Nucl. Chem.* 36, 1937-1946.

650   Cornell R.M. and Schwertmann U. (2003) *The Iron Oxides - Structure, Properties, Reactions,*

651   *Occurences and Uses*, Second Edition. Wiley-VCH, New York.

652   Cozar O., Leopold N., Jelic C., Chis V., David L., Mocanu A. and Tomoaia-Cotisel M.

653   (2006) IR, Raman and surface-enhanced Raman study of desferrioxamine B and its Fe(III)

654   complex, ferrioxamine B. *J. Mol. Struct.* 788, 1-6.

655   Cramer S.M., Bryon N. and Csaba H. (1984) High-performance liquid chromatography of

656   deferroxamine and ferrioxamine: interference by iron present in the chromatographic

657   system. *J. Chromatogr. A* 295, 405–411.

658   Dhungana S., White P.S. and Crumblis A.L. (2001) Crystal structure of ferrioxamine B: a

659   comparative analysis and implications for molecular recognition. *J. Biol. Inorg. Chem.* 8,

660   810–818.

661   Domagal-Goldman S.D., Paul K.W., Sparks D.L. and Kubicki J.D. (2009) Quantum chemical

662   study of the Fe(III)-desferrioxamine B siderophore complex - Electronic structure,

663   vibrational frequencies, and equilibrium Fe-isotope fractionation. *Geochim. Cosmochim.*

664   *Acta* 73, 1-12.

665   Dubbin W.E. and Ander E.L. (2003) Influence of microbial hydroxamate siderophores on

666   Pb(II) desorption from α-FeOOH. *Applied Geochemistry* 18, 1751-1756.

667   Edwards D.C., Nielsen S.B., Jarzecki A.A., Spiro T.G. and Myneni S.C.B. (2005)

668   Experimental and theoretical vibrational spectroscopy studies of acetohydroxamic acid

669   and desferrioxamine B in aqueous solution: Effects of pH and iron complexation.

670   *Geochim.Cosmochim. Acta* 69, 3237-3248.

671   Filius J.D., Lumsdon D.G., Meeussen J.C.L., Hiemstra T. and van Riemsdijk W.H. (2000)

672   Adsorption of fulvic acid on goethite. *Geochim.Cosmochim. Acta* 64, 51-60.

673   Filius J.D., Meeussen J.C.L., Lumsdon D.G., Hiemstra T. and van Riemsdijk W.H. (2003)

674   Modeling the binding of fulvic acid by goethite: the speciation of adsorbed FA molecules.

675   *Geochim.Cosmochim. Acta* 67, 1463-1474.

676   Fu H. and Quan X. (2006) Complexes of fulvic acid on the surface of hematite, goethite, and

677   akaganeite: FTIR observation. *Chemosphere* 63, 403-410.

678   Gan D., Kotob S.I. and Walia D.S. (2007) Evaluation of a spectrophotometric method for

679   practical and cost effective quantification of fulvic acid. *Ann. Environ. Sci.* 1, 11–15.

680   Ghabbour E.A. and Davies G. (2009) Spectrophotometric analysis of fulvic acid solutions - A

681   second look. *Ann. Environ. Sci.* 3, 131–138.

682   Haselwandter K. (2008) Structure and function of siderophores produced by mycorrhizal

683   fungi. *Mineral. Mag.* 72, 61-64.

684   Hay M.B. and Myneni S.C.B. (2007) Structural environments of carboxylic groups in natural

685   organic molecules from terrestial systems. Part 1: infrared spectroscopy.

686   *Geochim.Cosmochim. Acta* 71, 3518-3532.

687   Holmén B.A. and Casey W.H. (1996) Hydroxamate ligands, surface chemistry and the

688   mechanism of ligand promoted dissolution of goethite [α-FeOOH(s)].

689   *Geochim.Cosmochim. Acta* 60, 4403-4416.

690   Holmén B.A. and Casey W.H. (1998) Erratum to Hydroxamate ligands, surface chemistry

691   and the mechanism of ligand promoted dissolution of goethite [α-FeOOH(s)].

692   *Geochim.Cosmochim. Acta* 62, 726.

693   International Humic Substance Society (2008) FTIR spectra were measured at the Instituto di

694   Chimica Agraria, Università di Bari, Bari, Italy. [online] Available at:

695   <http://www.humicsubstances.org/spectra.html> [Accessed on 25th June, 2012].

696   Kosmulski M., Durand-Vidal S., Maczaka E. and Rosenholm J. (2004) Morphology of

697   synthetic goethite particles. *J. Colloid Interf. Sci.* 271, 261-269.

698   Kraemer S.M. (2004) Iron oxide dissolution and solubility in the presence of siderophores.

699   *Aquat. Sci.* 66, 3-18.

700   Kraemer S.M., Cheah S., Zapf R., Xu J., Raymond K.N. and Sposito G. (1999) Effect of

701   hydroxamate siderophore on Fe release and Pb(II) adsorption by goethite.

702   *Geochim.Cosmochim. Acta* 63, 3003-3008.

703   Lasaga A.C. (1998) *Kinetic Theory in the Earth Sciences*. Princeton University Press.

704   Liermann L.J., Kalinowski B.E., Brantley S.L. and Ferry J.G. (2000) Role of bacterial

705   siderophores in dissolution of hornblende. *Geochim.Cosmochim. Acta* 64, 587-602.

706   Muller F. and Batchelli S. (2011) Binding of iron and copper to humic colloids in the Thurso

707   River plume. *Geophys. Res. Abstr.* 13, EGU2011-8132.

708   Nightingale R.E., Wagner E.L. (1954) The vibrational spectra and structure of solid

709   hydroxylamine and deutero-hydroxylamine. *J. Chem. Phys.* 22, 203–207.

710   Pandeya S.B. (1993) Ligand competition method for determining stability constants of fulvic

711   acid iron complexes. *Geoderma* 58, 219–231.

712   Powell P.E., Cline G.R., Reid C.P.P. and Szanislo P.J. (1980) Occurrence of hydroxamate

713   siderophore iron chelators in soils. *Nature* 287, 833–834.

714 Prasad P.S.R., Prasad K.S., Chaitanya V.K., Babu E.V.S.S.K., Sreedhar B. and Murthy S.R.

715   (2006) In situ FTIR study on the dehydration of natural goethite. *J. Asian Earth Sci.* 27,

716   503-511.

717 Qu J.-H., Liu H.-J., Liu S.-X. and Lei P.J. (2003) Reduction of fulvic acid in drinking water

718   by ferrate. *J Environ. Eng.-ASCE* 129, 17-24.

719 Raymond K.N. and Dertz E.A. (2004) Biochemical and physical properties of siderophores.

720   In *Iron Transport in Bacteria* (eds. A.R. Mew, S.M. Payne and J.H. Crosa). ASM Press,

721   Washington, pp. 3 - 17.

722 Reichard P.U., Kretzschmar R. and Kraemer S.M. (2007a) Dissolution mechanisms of

723   goethite in the presence of siderophores and organic acids. *Geochim. Cosmochim. Acta* 71,

724   5635-5650.

725 Reichard P.U., Kretzschmar R. and Kraemer S.M. (2007b) Rate laws of steady-state and non-

726   steady-state ligand-controlled dissolution of goethite. *Colloid Surface A* 306, 22-28.

727 Ritchie J.D. and Perdue E.M. (2003) Proton-binding study of standard and reference fulvic

728   acid, humic acids, and natural organic matter. *Geochim. Cosmochim. Acta* 67, 85-96.

729 Schindler P.W. (1990) Co-adsorption of Metal Ions and Organic Ligands: Formation of

730   Ternary Complexes. In *Mineralogy Volume 23 Mineral-Water Interface Geochemistry*

731   (eds. M.F. Hochella and A.F. White). Mineralogical Society of America, Washington, DC.

732   Chapter 7.

733 Schwertmann U. and Cornell R.M. (1991) *Iron Oxides in the Laboratory: Preparation and*

734   *Characterisation.* VCH Publishers, New York.

735 Sharma B.K. (2007) *Fundamental Principles of Spectroscopy.* Krishna Prakashan Media Ltd,

736   Delhi.

737 Siebner-Freibach H., Hadar Y., Yariv S., Lapides I. and Chen Y. (2006)

738 Thermospectroscopic study of the adsorption mechanism of the hydroxamic siderophore

739 ferrioxamine B by calcium montmorillonite. *J Agric Food Chem.* 54, 1399-1408.

740 Simanova A.A., Persson P. and Loring J.S. (2010) Evidence for hydrolysis and Fe(III)

741 reduction in the dissolution of goethite by desferrioxamine-B. *Geochim.Cosmochim. Acta*

742 74, 6706-6720.

743 Sposito G. (1984) *The Surface Chemistry of Soils*. Oxford University Press, New York.

744 Sposito G. (1994) *Chemical Equilibria and Kinetics in Soils*. Oxford University Press, New

745 York. .

746 Stevenson R.J. (1985) Geochemistry of Soil Humic Substances. In *Humic Substances in Soil,*

747 *Sediment and Water- Geochemistry, Isolation and Characterisation* (eds. G.R. Aiken,

748 D.M. McKnight and R.L. Wershaw). John Wiley and Sons, New York.

749 Stumm W., Wehrli B. and Wieland E. (1987) Surface complexation and its impact on

750 geochemical kinetics. *Croat. Chem. Acta* 50, 1861-1869.

751 Tatár E., Mihucz V.G., Zámbó L., Gasparics T. and Záray G. (2004) Seasonal changes of

752 fulvic acid, Ca and Mg concentrations of water samples collected above and in the Béke

753 Cave of the Aggtelek karst system (Hungary). *Appl. Geochem.* 19, 1727-1733.

754 Tipping E. and Cooke D. (1982) The effects of adsorbed humic substances on the surface

755 charge of goethite (α-FeOOH) in fresh waters. *Geochim.Cosmochim. Acta* 46, 75-80.

756 Watteau F. and Berthelin J. (1994) Microbial dissolution of iron and aluminium from soil

757 minerals: efficiency and specificity of hydroxamate siderophores compared to aliphatic

758 acids. *Eur. J. Soil Biol.* 30, 1–9.

759 Weng L.P., Koopal L.K., Hiemstra T., Meeussen J.C.L. and Van Riemsdijk W.H. (2005)

760 Interactions of calcium and fulvic acid at the goethite-water interface.

761 *Geochim.Cosmochim. Acta* 69, 325-339.

762 Weng L.P., Van Riemsdijk W.H., Koopal L.K. and Hiemstra T. (2006) Adsorption of humic

763   substances on goethite: Comparison between humic acids and fulvic acids. *Environ. Sci.*

764   *Technol.* 40, 7494-7500.

765 Whitnall M. and Richardson D.R. (2006) Iron: A new target for pharmacological intervention

766   in neurodegenerative diseases. *Semin. Pediatr. Neurol.* 13, 186–187.

767

768

769

770

771

772

773

774

775

776

777

778

779

780

781

782

783

784

785

786

788

789   Figure 1. (a) Structural representation of desferrioxamine-B (DFOB). The terminating R

790   group (i) is an amine (pK$_a$ = 10.9). The three hydroxyl groups (ii – iv) have pK$_a$ values of 9.8,

791   9.2 and 8.6, respectively (Colnaghi Simionato et al., 2006). The hydroxamate (oxime) group

792   is shown along with the amide I (C=O) and amide II (N-H and C-N). Adapted from Whitnall

793   and Richardson (2006). (b) Structure of DFOB bound to Fe^{3+} as ferrioxamine B. DFOB is

794   hexadentate, giving a complex with Fe^{3+} comprised of three, five-membered rings. Adapted

795   from Cramer et al. (1984).

796

797   Figure 2. Generalised depiction of the proposed molecular structure of FA based on the

798   Temple-Northeastern-Birmingham (TNB) molecular modelling programme (Alvarez-Puebla

799   et al. (2006), in accordance with the experimentally derived elemental composition, number

800   and type of acidic groups, and molecular weight of FA.

801

802   Figure 3. Graphical representation showing the permutations of the batch dissolution of

803   goethite with DFOB and SRFA as a function of reaction duration.

804

805   Figure 4. Iron release by goethite in the presence of only DFOB (system 1) and both DFOB

806   and SRFA (systems 2 – 6), with permutations as described in Fig. 3. System 7 is a goethite-

807   SRFA suspension; system 8 is a goethite suspension lacking any organic ligand. Systems 9

808   and 10 are solutions of DFOB and SRFA, respectively, and serve as controls. Initial

809   siderophore concentration: 270 μM; solid concentration: 0.7 g L^{-1}; pH 6.5.

810

811

812

Figure 5. UV-Vis spectra of untreated filtrate solutions showing absorbance for uncomplexed

DFOB (270 μM) near 236 nm and absorbance for the Fe-DFOB complex appearing as a low,

broad peak at 400 – 500 nm.

816

Figure 6. FTIR spectra for synthetic goethite, DFOB, SRFA, Fe-DFOB, Fe-SRFA, DFOB-

SRFA and Fe-DFOB-SRFA. Reference compounds have the following molar ratios:-

Fe:DFOB (2:1), Fe:SRFA (5:1), DFOB:SRFA (1:1) and Fe:DFOB:SRFA (5:1:1). See Table

2 for peak assignments.

821

Figure 7. Schindler diagrams illustrating the charge properties of goethite and ionic SRFA

and DFOB. The horizontal bar in the bottom rectangle indicates the pH range over which

purely electrostatic adsorption mechanisms are possible.

825

Figure 8. Proposed adsorption mechanism for the goethite-SRFA complex, involving a

chelate ring incorporating COO^- and phenolic OH from SRFA.

828

Figure 9. Proposed mechanism of goethite dissolution in the presence of DFOB and SRFA.

830

831

Table 1

Table 1. Linear regression equations, mass-normalised zero-order dissolution rate coefficients, surface excess values for DFOB, and pseudo-first-order rate coefficients for goethite dissolution at pH 6.5 and 25°C.

System	Regression equation	Rate coefficient (μmol g^{-1} h^{-1})	DFOB surface excess (μmol g^{-1})	Pseudo-first-order rate coefficient (h^{-1})
1	Y = 0.180X + 11.90	0.257 ± 0.016	14.4	0.018
2	Y = 0.191X + 14.94	0.273 ± 0.009	19.0	0.014
3	Y = 0.188X + 10.00	0.268 ± 0.034	23.3	0.012
4	Y = 0.255X + 14.66	0.364 ± 0.014	18.3	0.020
5	Y = 0.289X + 14.08	0.412 ± 0.000	26.5	0.016
6	Y = 0.308X + 29.72	0.440 ± 0.070	22.8	0.019

Initial DFOB concentration = 270 μM
Goethite concentration = 0.7 g L^{-1}
Y = soluble Fe (μM)
X = time (h)

Table 2

Table 2. FTIR absorption bands (cm^{-1}) and their assignments for DFOB, synthetic goethite, SRFA and four complexes: Fe-DFOB, Fe-SRFA, DFOB-SRFA and Fe-DFOB-SRFA. Assignments are based on Cornell and Schwertmann (2003); Edwards et al. (2005); Cozar et al. (2006); Prasad et al. (2006); and Borer et al. (2009). Vibration modes are designated as follows: ν, stretching; δ, deformation; s, symmetrical; as, asymmetric.

Assignment	DFOB	Goethite	SRFA	Fe-DFOB	Fe-SRFA	DFOB-SRFA	Fe-DFOB-SRFA
$\nu_{C=O}$ amide I	1624			1622		1624	
$\nu_{C=O}$ hydroxamate	1599						
$\nu_{C=N}$ hydroxamate (resonance)				1568			
δ_{N-H}, ν_{C-N} amide II	1537						
δ_{NOH}, ν_{C-N}, ν_{C-N} hydroxamate X2, adjacent to hydroxamate	1480						
ν_{Fe-O} hydroxamate-iron				1459			
ν_{C-N}, δ_{C-H}, δ_{N-H} hydroxamate X2, terminal N	1386						
ν_{N-O} hydroxamate (resonance)	1047			1045		1046	1042
ν_{Fe-O} hydroxamate-iron				561			542
ν_{OH} (phenolic)			3425		3410	3417	3437
ν_{N-H} (terminal N)	3128 3325			3368		2939	3010 2954
$\nu_{C=O}$ carboxylic acid protonated			1720		1687	1719	1723
$\nu_{as\,C=O}$ carboxylic acid deprotonated			1629		1631	1626	1642
$\nu_{s\,C=O}$ carboxylic acid deprotonated			1384		1384	1385	
ν_{OH} phenolic			1218			1218	1216
$\nu_{(OH)}$ hydroxyl stretch		3132					
δ_{OH} in-plane-hydroxyl		891					
δ_{OH} out-of-plane hydroxyl		795					
ν_{FeO6} lattice mode		640					

Figure 1
Click here to download high resolution image
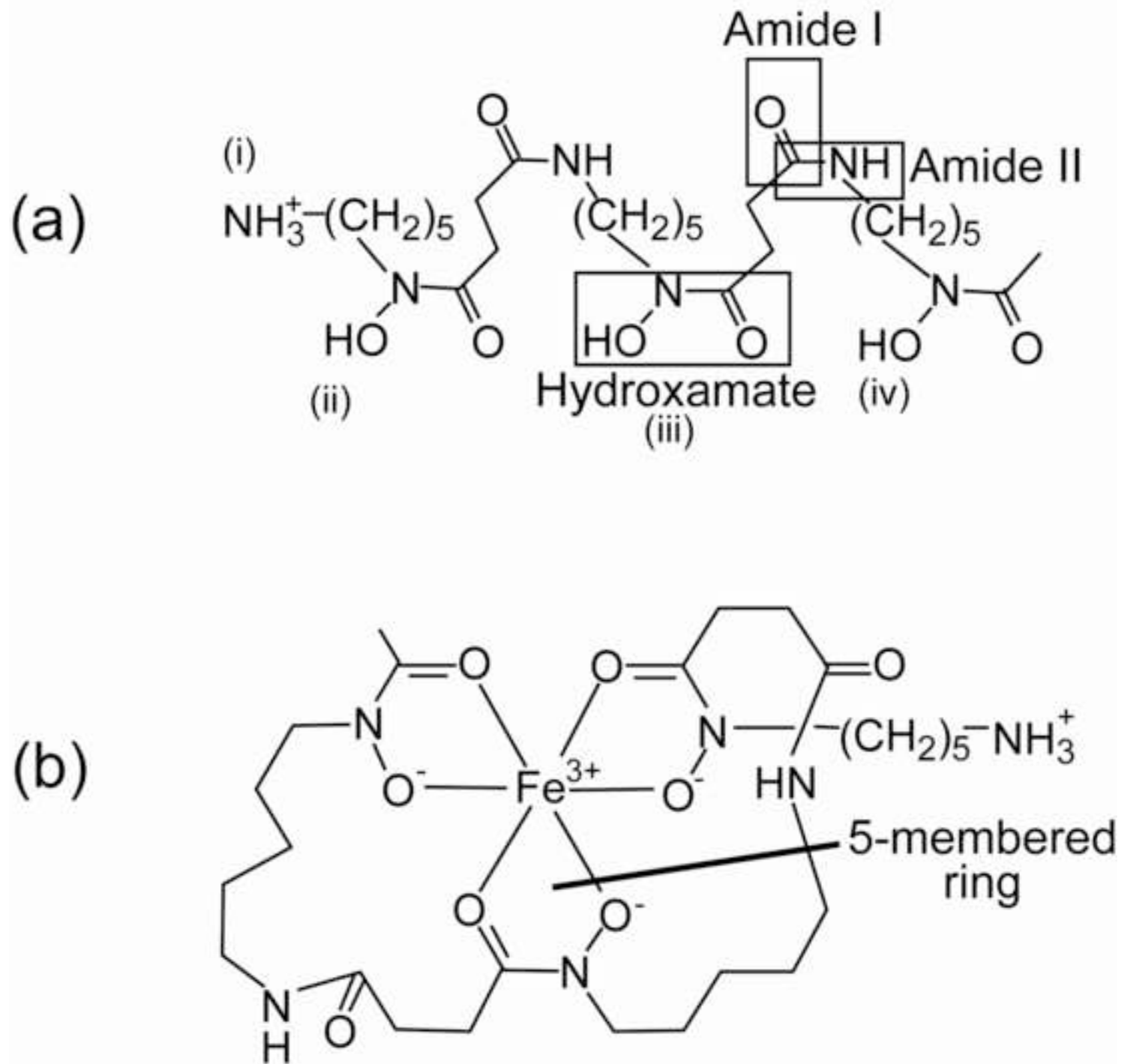
Figure 1

Figure 2
Click here to download high resolution image
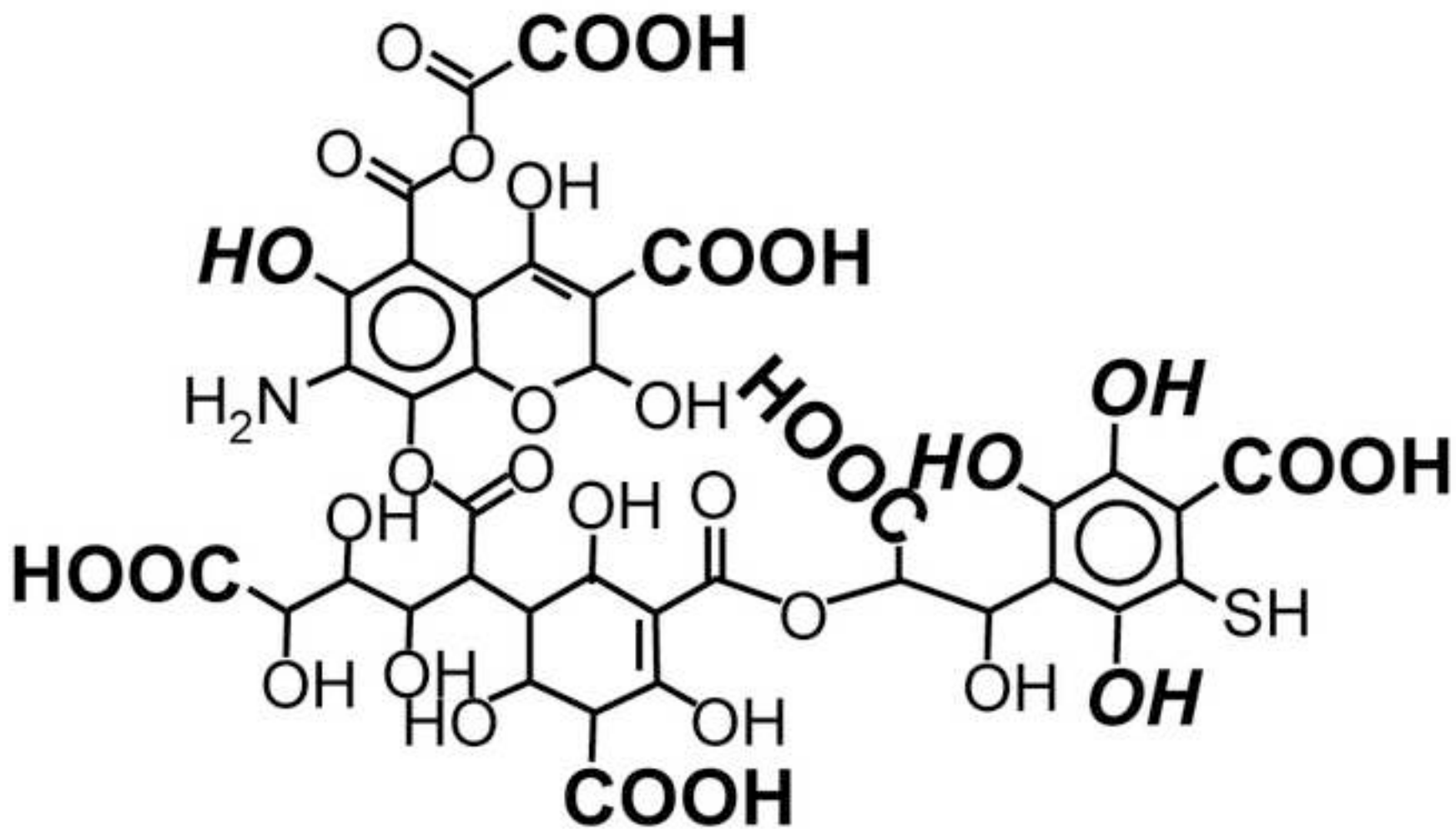
Phenolic group: $(C_6H_5)OH, HO(H_5C_6)$

Carboxylic acid group: COOH, HOOC

Figure 3
Click here to download high resolution image
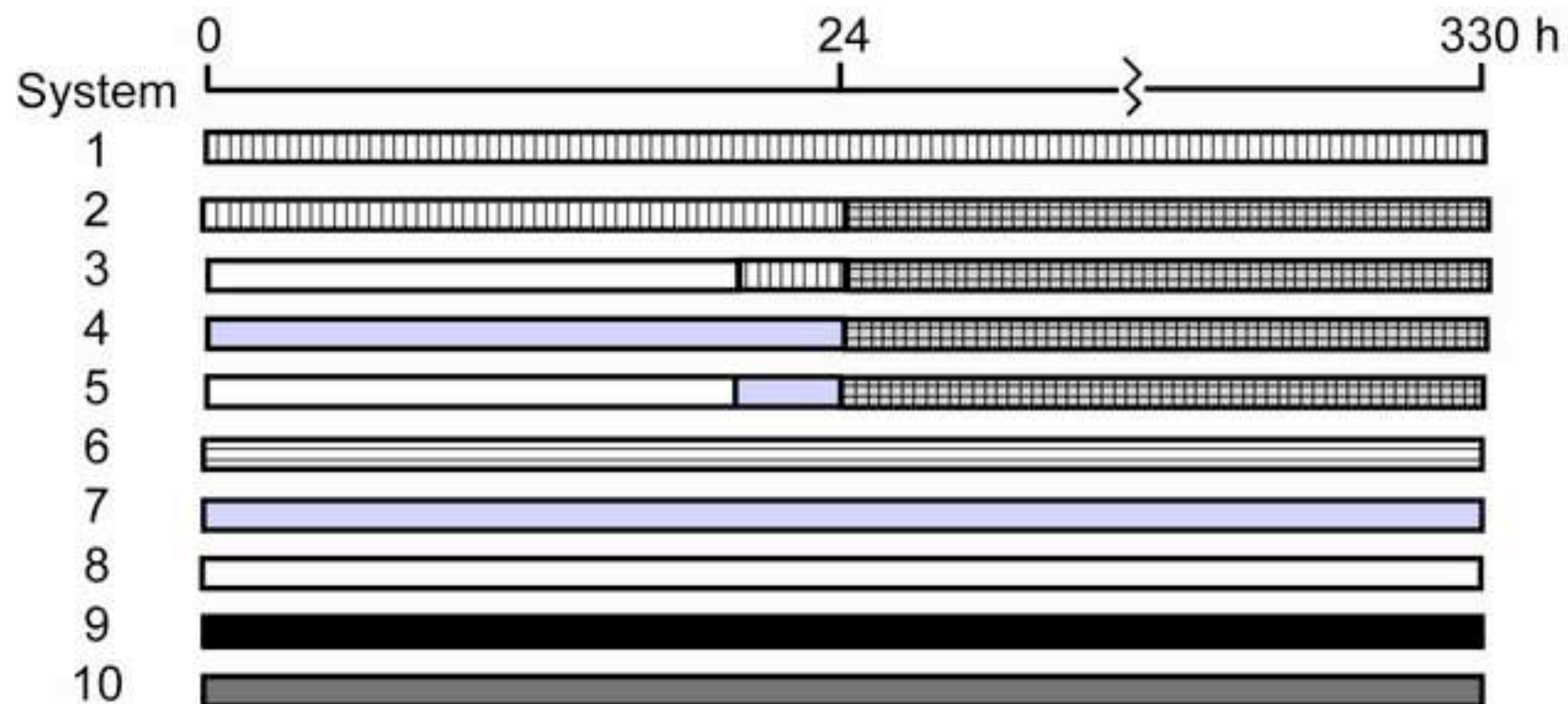
Figure 3

Figure 4
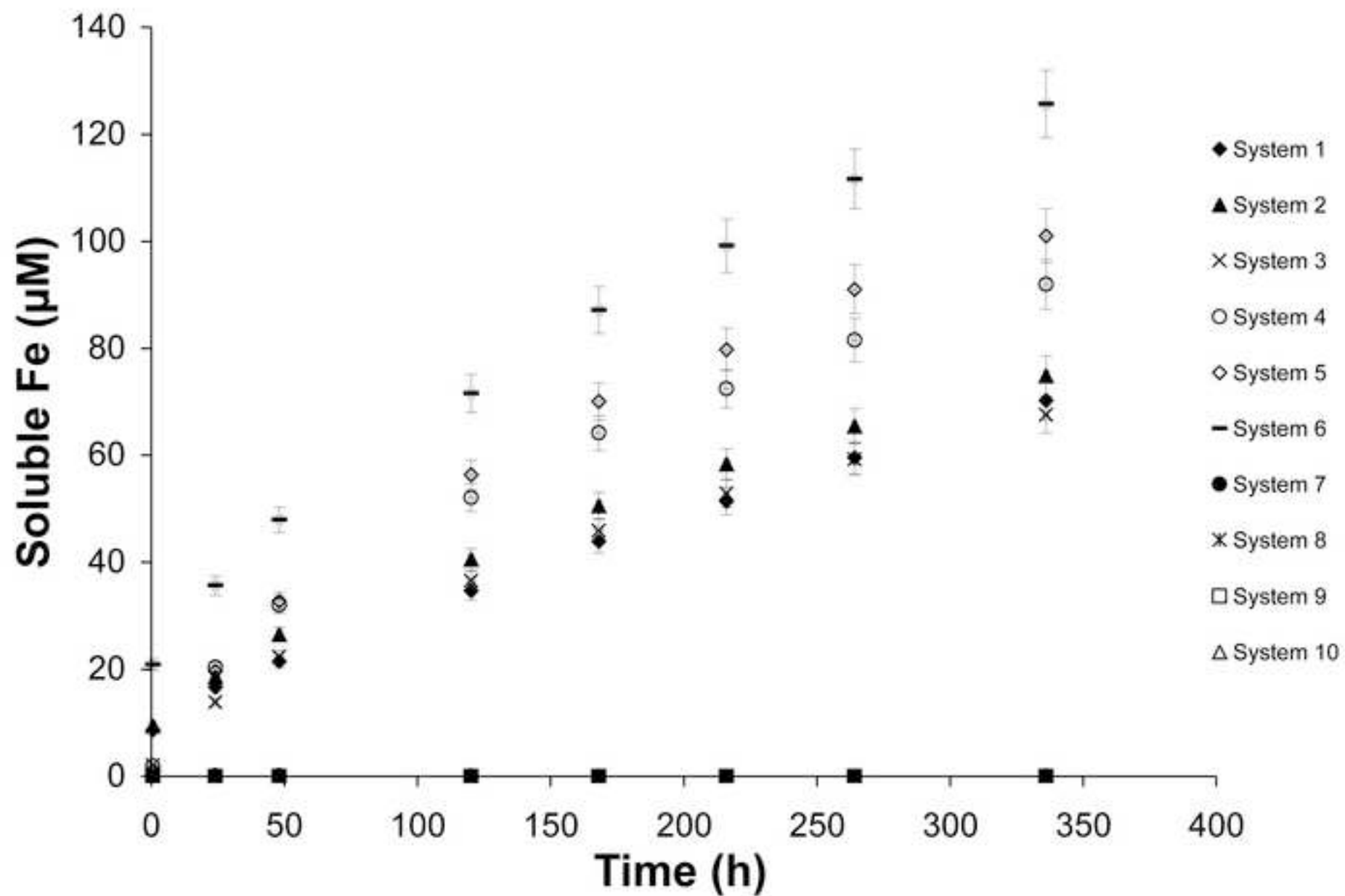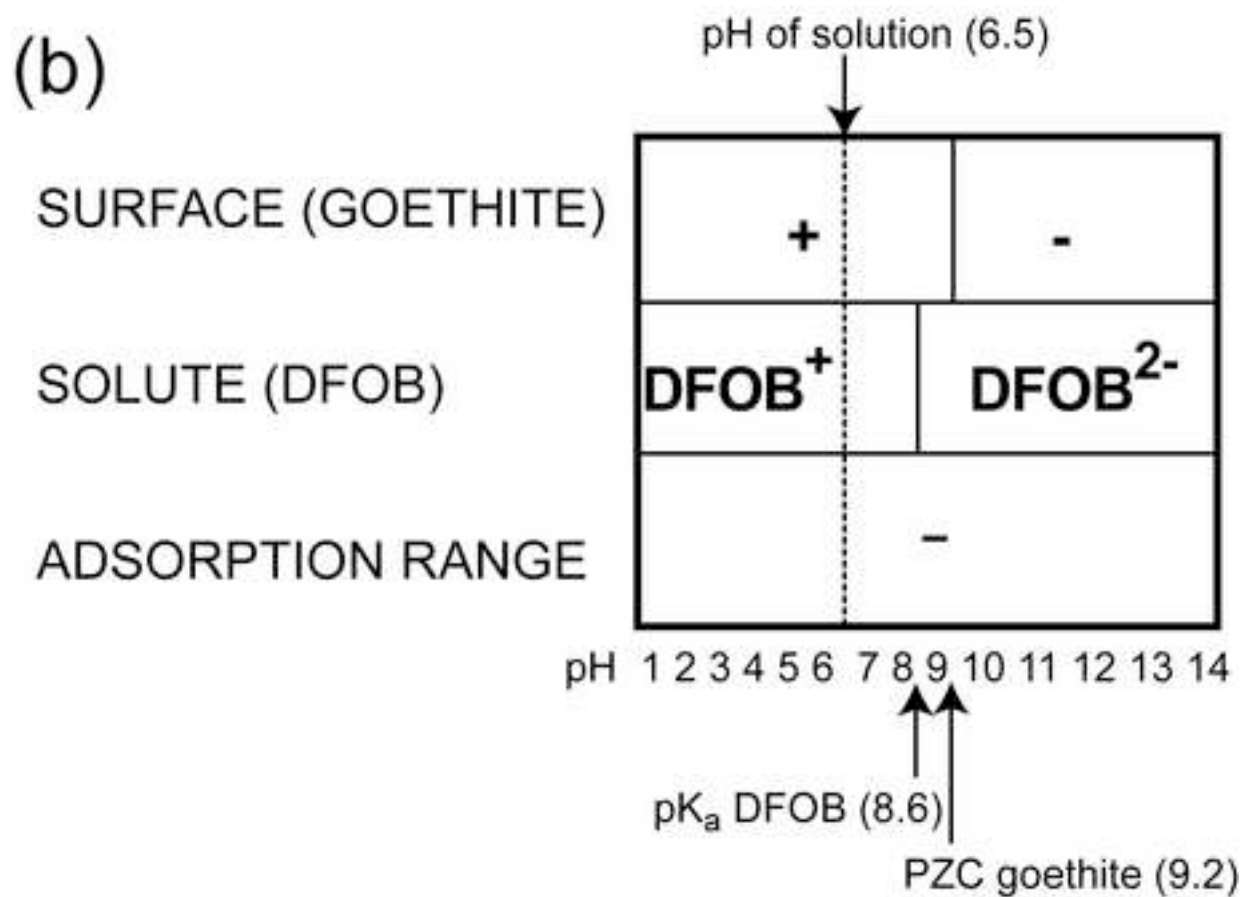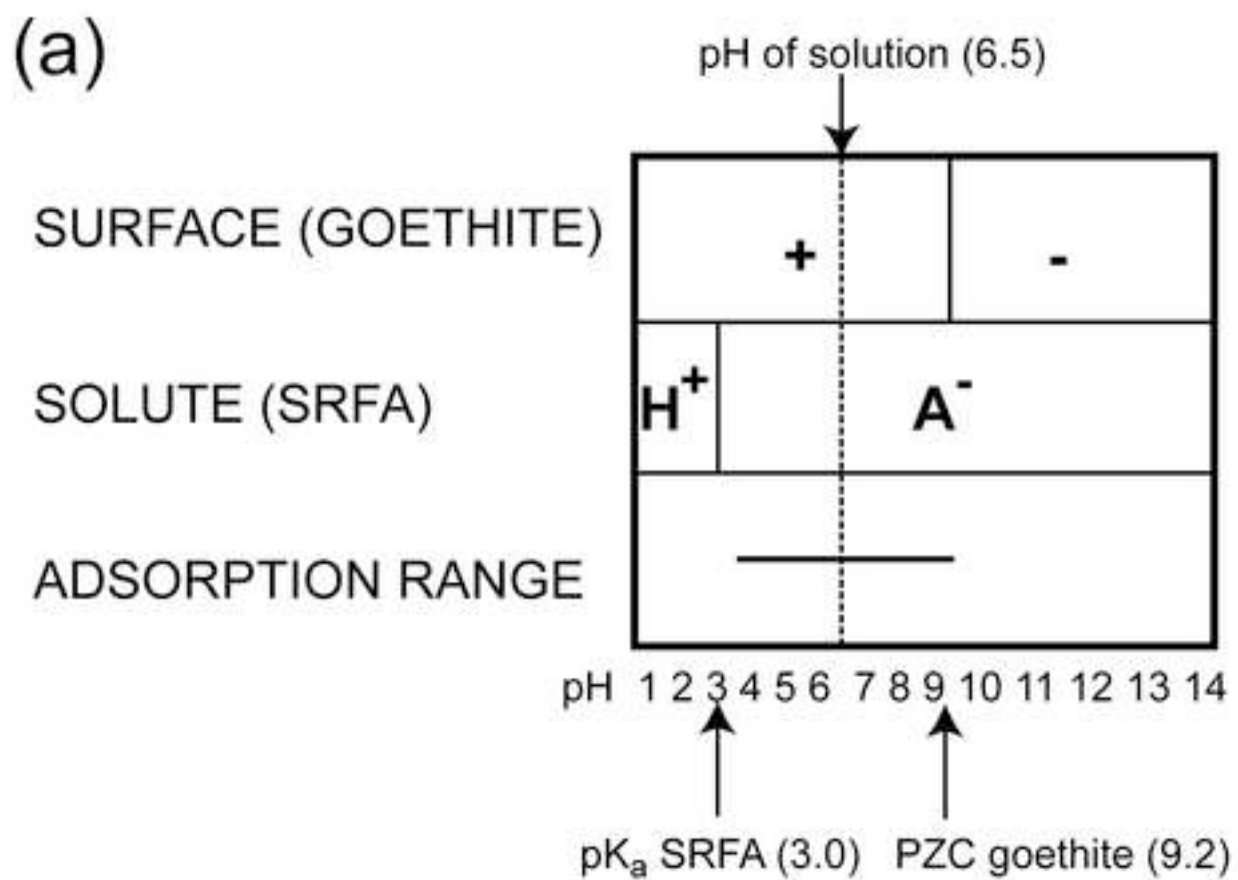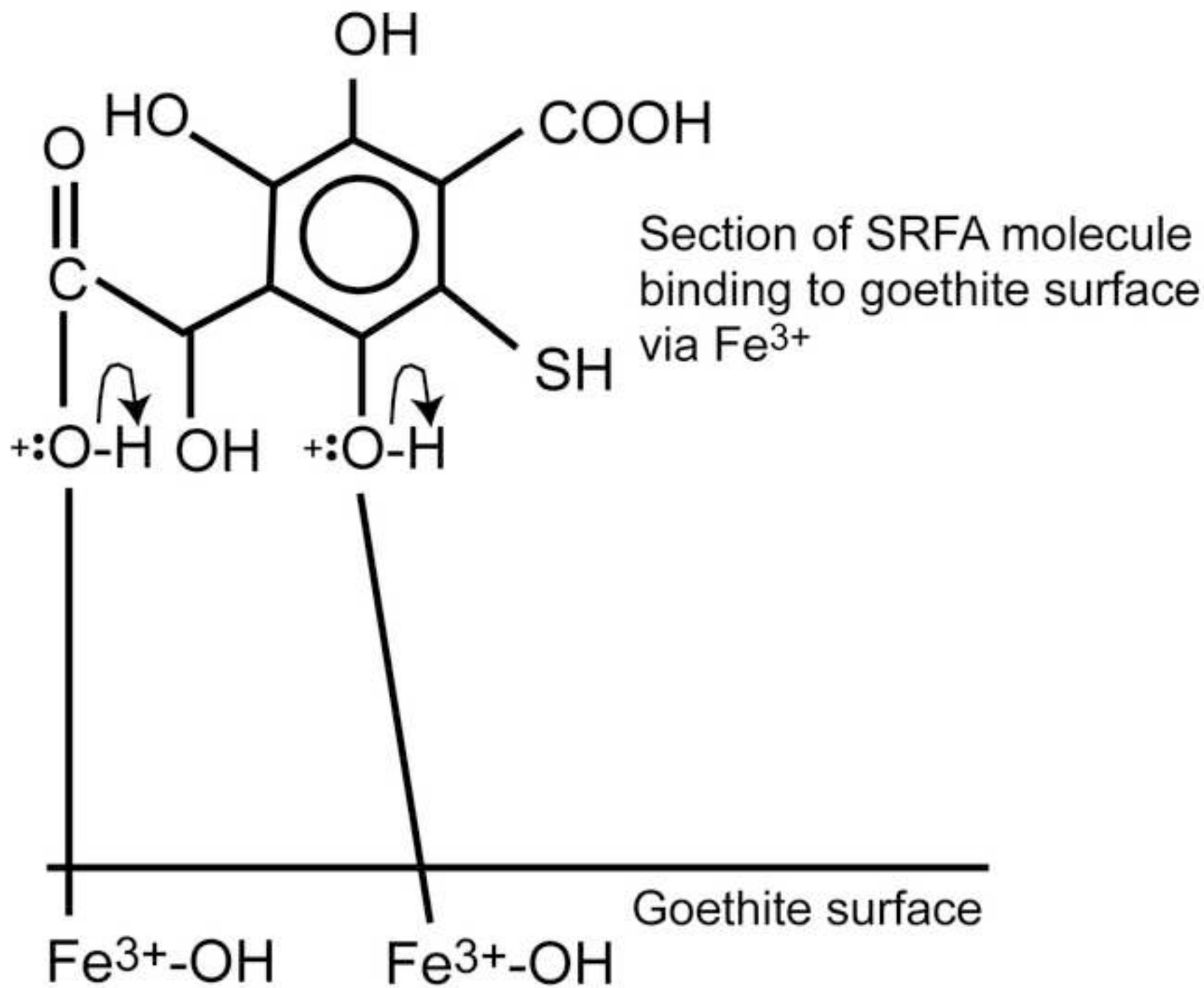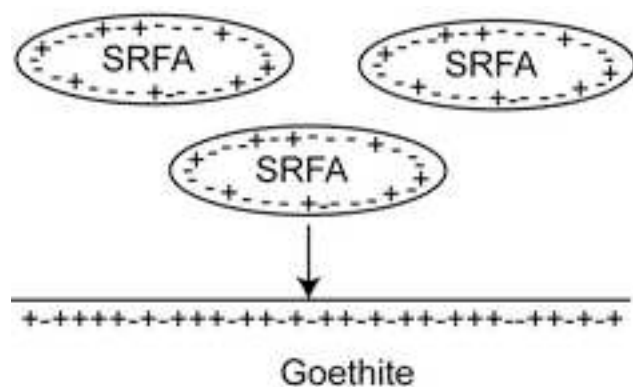**Click here to download high resolution image**

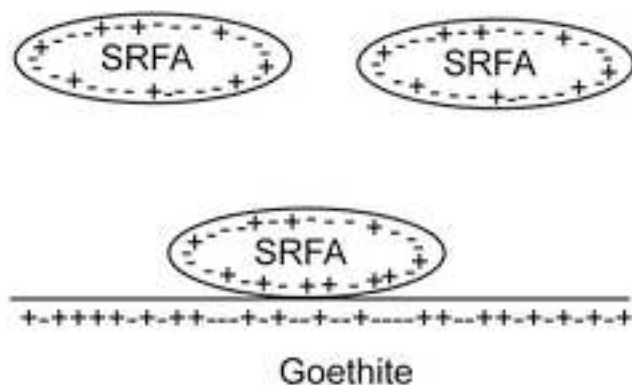Figure 5
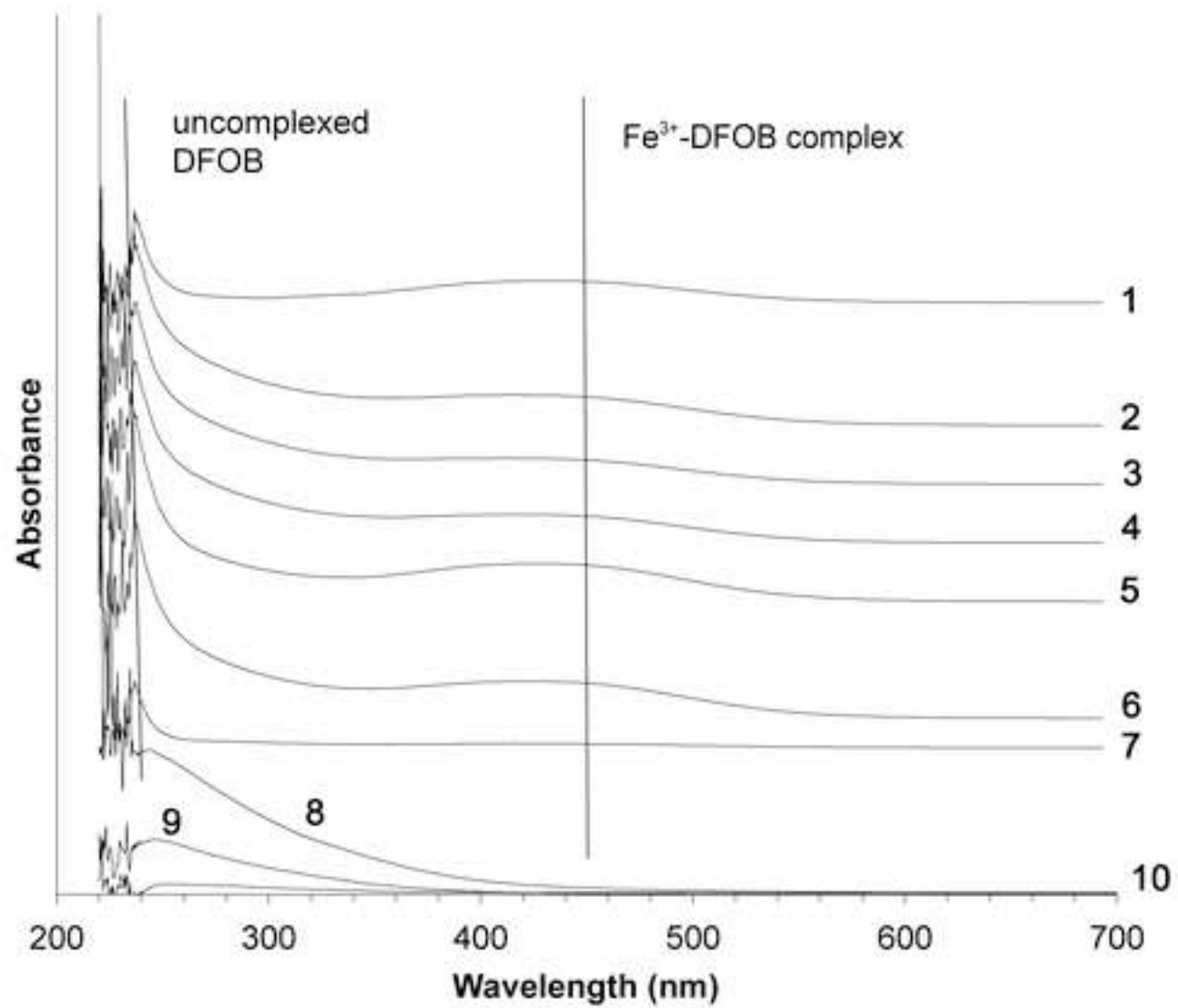
Figure 6
[Click here to download high resolution image](#)
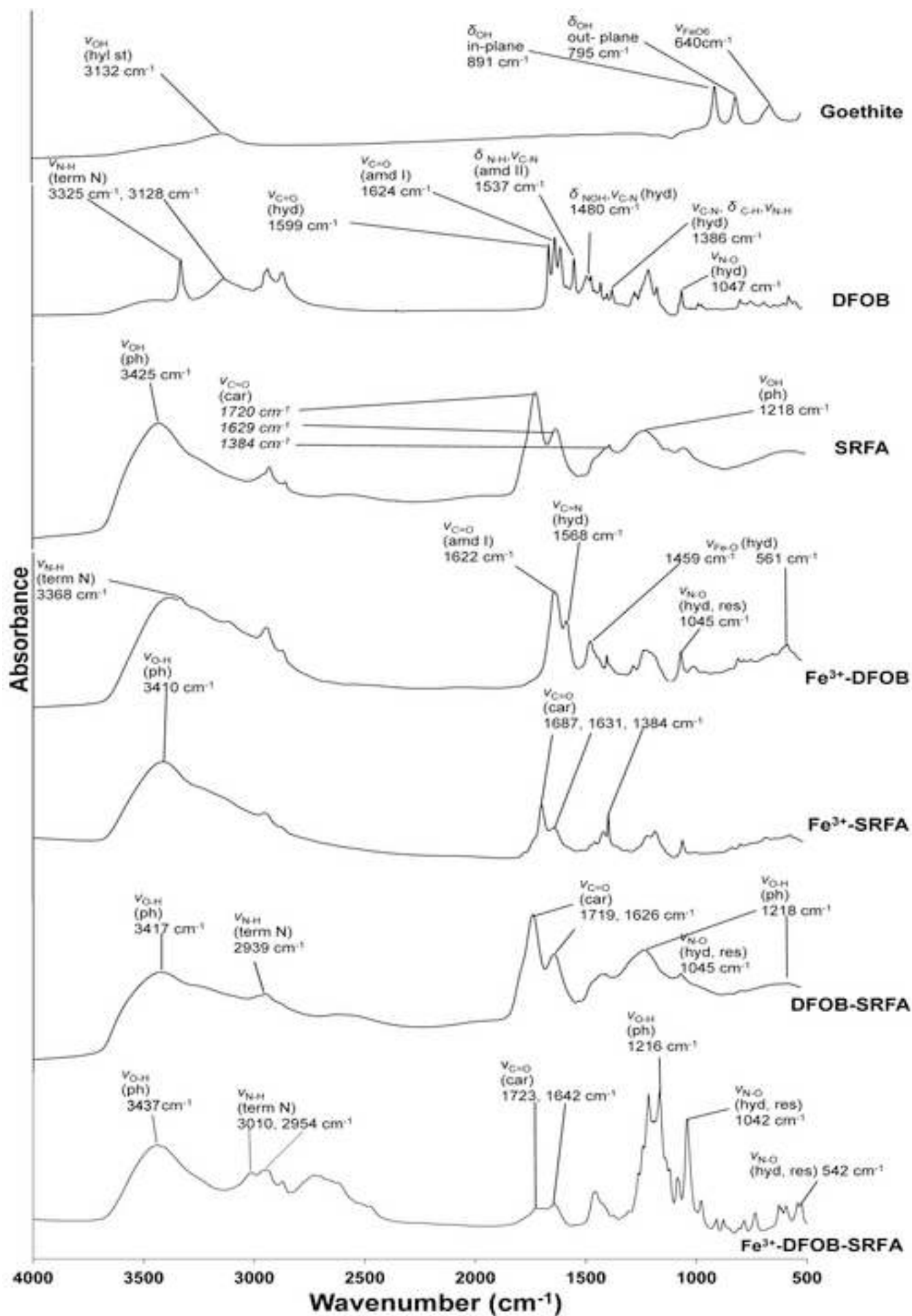
Figure 6

Figure 7

Figure 8
Click here to download high resolution image

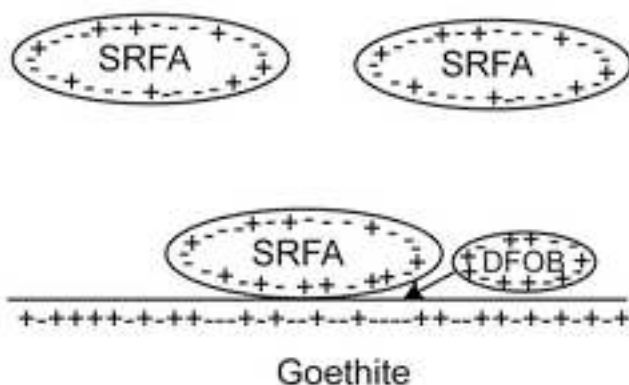Section of SRFA molecule binding to goethite surface via Fe^{3+}

Figure 9
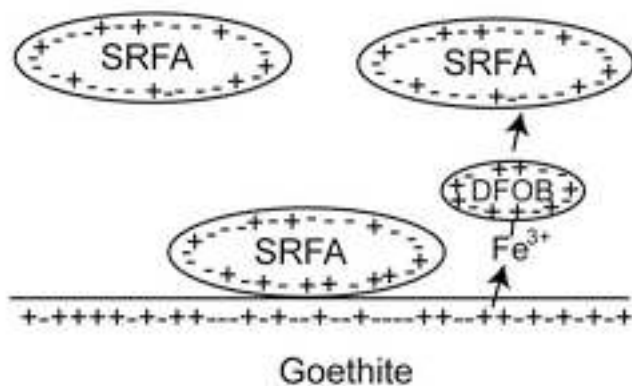[Click here to download high resolution image](#)

Step 1. At pH 6.5, SRFA surface is negatively charged, and goethite surface is positively charged.

Step 2. Areas on the goethite surface become less positive in the vicinity of the SRFA molecule.

Step 3. The hydroxamate furthest from the protonated amine in the DFOB bonds to the less positive areas on the goethite surface.

Step 4. DFOB bonds with Fe^{3+} on the goethite surface. The new Fe^{3+}-DFOB complex then detaches from the surface into solution and approaches other SRFA molecules.